Seismic Tomography 2024

Andreas Fichtner[1], Brian L. N. Kennett[2], Victor C. Tsai[3], Clifford H. Thurber[4], Arthur J. Rodgers[5], Carl Tape[6], Nicholas Rawlinson[7], Roger D. Borcherdt[8], Sergei Lebedev[7], Keith Priestley[7], Christina Morency[5], Ebru Bozdağ[9], Jeroen Tromp[10], Jeroen Ritsema[11], Barbara Romanowicz[12], Qinya Liu[13], Eva Golos[4], Fan-Chi Lin[14]

[1]Department of Earth Sciences, ETH Zurich, Zurich, Switzerland
[2]Research School of Earth Sciences, The Australian National University, Canberra, Australia
[3]Department of Earth, Environmental and Planetary Sciences, Brown University, Providence RI, USA
[4]Department of Geoscience, University of Wisconsin-Madison, Madison, WI, USA
[5]Lawrence Livermore National Laboratory, Livermore, CA, USA
[6]University of Alaska Fairbanks, Fairbanks, AK, USA
[7]Department of Earth Sciences, University of Cambridge, Cambridge, United Kingdom
[8]U. S. Geological Survey, Menlo Park, CA, USA
[9]Department of Applied Mathematics & Statistics and Department of Geophysics, Colorado School of Mines, Golden, CO, USA
[10]Department of Geosciences and Program in Applied & Computational Mathematics, Princeton University, Princeton, NJ, USA
[11]Earth & Environmental Sciences, University of Michigan Ann Arbor, MI, USA
[12]Department of Earth and Planetary Science, University of California at Berkeley, Berkeley, CA, USA
[13]Department of Physics & Department of Earth Sciences, University of Toronto, Toronto, Canada
[14]Department of Geology and Geophysics, University of Utah, Salt Lake City, UT, USA

Key Points:

- This Special Issue introduction documents opinions on major challenges and promising research directions.
- Although no efforts were made to align these opinions, a small number of topics emerge as outstanding issues.
- This article is intended to be a resource for both established and early-career scientists.

Corresponding author: Andreas Fichtner, andreas.fichtner@erdw.ethz.ch

Abstract

Seismic tomography is the most abundant source of information about the internal structure of the Earth, at scales ranging from a few meters to thousands of kilometers. It constrains the properties of active volcanoes, earthquake fault zones, deep reservoirs and storage sites, glaciers and ice sheets, or the entire globe. It contributes to outstanding societal problems related to natural hazards, resource exploration, underground storage, and many more. Recent advances in seismic tomography are being translated to non-destructive testing, medical ultrasound and helio-seismology. Nearly 50 years after its first successful applications, this paper offers a snapshot of modern seismic tomography. Focused on major challenges and particularly promising research directions, it is intended to guide both Earth science professionals and early-career scientists. The individual contributions by the co-authors provide diverse perspectives on topics that may at first seem disconnected, but are in fact closely tied together by a few coherent threads: multi-parameter inversion for properties related to dynamic processes, data quality and geographic coverage, uncertainty quantification that is useful for geologic interpretation, new formulations of tomographic inverse problems that address concrete geologic questions more directly, and the presentation and quantitative comparison of tomographic models. It remains to be seen which of these problems will be considered solved, solved to some extent, or practically unsolvable over the next decade.

Introduction

Seismic tomography is the art of translating recordings of seismic waves into quantitative images of the Earth's interior. Conceptualized nearly 50 years ago (e.g., Aki & Lee, 1976; Dziewoński et al., 1977; Aki et al., 1977), the family of seismic tomography methods has grown and diversified rapidly, thereby evolving into one of the cornerstones of geoscience. Seismic tomography reveals the dynamics and composition of the Earth and other planetary bodies, illuminates the structure of active volcanoes and fault zones, constrains the internal flow patterns of glaciers and ice sheets, provides information on deep reservoirs and storage sites, and enables the accurate simulation of earthquake-induced ground motion - to list just a few of its most prominent uses.

This broad impact of modern seismic tomography is rooted in a long series of developments that produce Earth models with continuously improving spatial resolution

and increasingly tighter constraints on seismic properties that are closely related to dynamic processes such as attenuation, anisotropy, poro-elasticity or the topography of internal discontinuities. Most of these developments, traced in several books and review articles (e.g., Iyer & Hirahara, 1993; Nolet, 2008; Fichtner, 2010; Q. Liu & Gu, 2012; Ringler et al., 2022), fall into one of four categories: (1) improvements in data coverage and quality, often related to novel instrumentation, (2) reductions of forward and inverse modelling errors through theoretical and numerical advances, (3) innovative data processing methods, including methods to extract targeted information from seismic data, and (4) the exploitation of increased computational power and novel hardware.

Despite the success and maturity of seismic tomography, our knowledge still requires substantial improvements in order to address both academic questions concerning the thermo-chemical state of the Earth and burning societal needs. The latter relate, for instance, to earthquake and volcanic hazards, geothermal energy exploration and production, long-term underground storage of hazardous materials and energy sources, as well as natural resource exploration and management.

Within this context, the most pertinent challenges and most promising research directions in seismic tomography were chosen to be the focus of a dedicated meeting organized by the Seismological Society of America that took place in October 2022 in Toronto, Canada. This introductory paper to the BSSA Special Section on *Modern Seismic Tomography* is a condensate of the Toronto meeting. It portrays the state of the art and contains opinions by long-term practitioners and developers on what the outstanding challenges and exciting topics for the next decade should be. They include complete reformulations of seismic tomography, multi-parameter inversion of more diverse datasets, uncertainty quantification and fundamental limitations of tomography, as well as advances and recommendations on Earth model presentation and interpretation. The content is deliberately unfiltered to ensure that potentially different opinions can be represented. Rather than offering a discussion or review, the text is intended to provoke discussions and critical reflections.

The contributions to this BSSA Special Section explore many of the directions covered in this opinion paper. Proposals of novel forward and inverse modelling approaches, for example, can be found in the works of Lebedev et al. (2024), Del Piccolo et al. (2024) and Borcherdt (2024). Lebedev et al. (2024) implement seismic thermography, by mak-

ing plausible assumptions on mantle composition and extracting information from noisy surface wave data to directly constrain temperature variations. Del Piccolo et al. (2024) extend transdimensional tomography to imaging anisotropy in the upper mantle, thereby quantifying the delicate balance between increasing model uncertainties and the need to incorporate additional parameters to describe anisotropic velocity variations. Borcherdt (2024) reviews exact viscoelastic ray-tracing algorithms that quantify ray trajectory perturbations across anelastic boundaries and effects of anelasticity on seismic tomography models.

Two of the contributions are concerned with the construction of multi-scale seismic Earth models. Lyu et al. (2024) introduce a numerical wave propagation approach for accurately coupling highly-resolved local domains and lower-resolution global-scale models in the context of box tomography. This is complemented by the work of Zhou et al. (2024), who propose a method for seismic velocity model fusion based on a probability graph method that avoids the introduction of artifacts and the suppression of small-scale structure.

Several papers exploit either very large data volumes or newly collected data to make concrete inferences about Earth structure and dynamics. Using ambient noise tomography, Lv et al. (2024) suggest that mid-lower crustal flow and NE subduction of the Indian Plate control deformation of the eastern Himalayan syntaxis, which is the leading edge of the Indian-Asian collision. Perugu et al. (2024) image the Andaman-Nicobar subduction zone using ocean-bottom seismometer data and reveal mantle upwellings, as well as volcanism-related low-velocity regions. Civiero et al. (2024) employed over 1.17 million Rayleigh and 300,000 Love-wave fundamental-mode phase-velocity measurements in the 17-310 s period range to constrain 1D upper-mantle models averaged over the globe and for eight distinct tectonic environments. One of the robust features is a distinct flip in the sign of global radial anisotropy from positive (Vsh > Vsv) to negative at 200-300 km depth.

Three novel full-waveform inversion models complete this Special Section. Carmona et al. (2024) extract frequency-dependent phase and amplitude information to constrain wave speeds and shear attenuation beneath the Arabian plate, thereby shedding light onto the origin of Cenozoic volcanism in the western Arabian Peninsula. Partly overlapping with their study region, Rodgers et al. (2024) present a radially anisotropic model

of the Middle East and Southwest Asia. The model constrains numerous regional tectonic features, and is shown to be sufficiently robust to help improve earthquake hazard analyses and explosion monitoring. Last but not least, Thrastarson et al. (2024) combine stochastic mini-batch optimization and wavefield-adapted spectral-element meshes to reduce the computational cost of a quasi-Newton iteration by more than two orders of magnitude, compared to standard full-waveform inversion. This drastic cost reduction enables the inversion of more than 6 million three-component waveform recordings from 2366 earthquakes, leading to their final global-scale model REVEAL.

This introductory paper is organized as a sequence of short contributions, each written by one of the co-authors on one or several topics that they find most relevant or challenging. As far as possible, the contributions are ordered and loosely grouped according to their particular focus. In the final section, we attempt to summarize some coherent threads that emerge, despite the remarkable diversity of the contributions.

INFERENCE, DATA QUALITY, AND ALTERNATIVES (Victor C. Tsai)

In my view, the most important directions for the future of seismic tomography are (1) to frame tomography to be better able to make clear, robust inferences about the Earth's interior in a practically useful manner, (2) to improve data quality and quantity, and (3) to diversify the approaches, tools and datasets used. While other directions are still worthwhile to pursue, I believe it is of lesser importance to focus on areas such as the improved accuracy of synthetics, computational efficiency, and machine learning that are the current focus of many researchers.

Robust, Practical Inference from Imaging: Given the limitations of geophysical data, the vast majority of tomographic results require significant smoothing or regularization to achieve unique answers (Jackson, 1972). One main reason for this is an implicit philosophy taken favoring flexible, mathematically convenient parameterizations such as grid cells, pixels, spherical harmonics or splines. Unfortunately, due to the regularization, such flexible 'discovery oriented' parameterizations do not achieve physically realistic results, and it is typically impossible to truly falsify any interpretations of features due to the qualitative nature of such interpretations. Since geophysical data will always be limited (even with progress in direction (2)), I suggest that the most progress would be made by making tomographic inversions more 'inference oriented', by inverting for simplified but physically reasonable models for the geological structures of potential interest that are uniquely determined without regularization. Within such an inference framework, multiple alternative hypotheses could be tested by running multiple inversions and using a model selection process (Sambridge et al., 2006; Vehtari et al., 2017). This general practical inference direction is discussed in significantly more detail in Tsai et al. (2023) and Tsai (2023).

Data Quality and Quantity: The severe under-sampling of information from the Earth's interior is partly due to data quality and quantity. Not only are there very few seismic stations in the oceans for obvious cost reasons, but there are also few openly accessible stations in Russia and Africa for various political and logistical reasons, leading to large areal coverage gaps (IRIS, 2018). Improving this coverage is crucial for deep Earth tomography to yield useful constraints. Equally importantly, however, is data quality. Unfortunately there has been a recent trend towards cheaper and lower quality seismic stations due to interest in differential measurements (and also with the hope that $\sqrt{N}$ stack-

ing can overcome the quality limitations). However, the abundant uncertainties and structural biases that arise due to low quality station installations and instruments often prevents tomographers from understanding which uncertainties are 'true' uncertainties related to deep Earth structure and which are due to local (sometimes extremely local) site issues, making the observations depart significantly from the typically assumed weakly attenuating elastic Earth.

Diversification of Approaches and Data Types: While many researchers would argue that convergence to standard methodologies and datasets is a useful goal, there is a danger of over-reliance on a standard set of tools and data. In global tomography, much fanfare has been given to the fact that many global mantle models are starting to agree on certain broad features of the deep mantle (Cottaar & Lekic, 2016). While this is a major step forward from the previous generation of global tomographic models, an important question is how much of this agreement is related to using similar datasets and similar methodologies. Currently, this question cannot be answered due to the significant overlap in all methodologies and data used for the compared models. This underscores the need for high-quality alternatives to standard approaches to utilizing the same data, as well as novel datatypes that are truly independent of the seismic data. I advocate for alternatives to standard adjoint frameworks that are nonetheless physically and mathematically justified, for example using frameworks where improvements in misfit are accomplished through different paths in model space (Haney & Tsai, 2015, 2017). For data types, while it is difficult for other data to achieve the resolution of seismic data, it will be crucial to test seismically inferred models of Earth's interior with neutrino (Donini et al., 2019), muon (Tanaka et al., 2009), electromagnetic (Naif et al., 2013), gravity (Oldenburg, 1974), and geodetic (Park et al., 2023) data that have different sensitivities and biases from the seismic data. While joint inversions with multiple data types are becoming more popular, these do not help test the robustness of the obtained images. Truly independent data must be left out of prospective tests to ensure against data dredging problems (Nuzzo, 2014; Wasserstein & Lazar, 2016).

THE IMPORTANCE OF INVERTING FOR WHAT WE REALLY WANT TO KNOW (Sergei Lebedev)

What is the goal of seismic tomography? To yield inferences on the structure and dynamics of Earth, as most Earth scientists would see it. For some applications, such as earthquake source or ground motion studies, models of the distribution of seismic velocities are what is needed. But for those concerned with Earth structure and dynamics, key properties of interest include temperature (T), composition, density, and movements of the rock at depth. Tomography is a quest for information, to paraphrase Tarantola and Valette (1982). With tomography's goals in mind, it must be a quest for information on what we want to know (T, etc.). This is a perilous quest, with treacherous pitfalls. Settle for a non-unique model half-way, build inferences on its poorly constrained features, and end up with implausible results and all useful information lost.

We can avoid losing information in the non-uniqueness of intermediate solutions by establishing direct quantitative relationships between the data and the inferences of interest (see also Tsai et al., 2023). Inverting seismic data directly for temperature and density, or temperature and composition, has been discussed in the field for decades. Yet, implementing this approach has challenges, and the field has generally stuck with the tried-and-tested one instead: let us not risk increasing errors by introducing potentially uncertain temperature-wave speed relationships; let us do what we know well and build best possible seismic-velocity models. The concerns are valid, and solving for T, etc., is not straightforward. Yet, the consequences of not inverting for what we really want to know are the loss of information from seismic data, failure to incorporate relevant information from other data types, and other setbacks in our quest for information.

New opportunities. Tomography has come a long way in its 40+ years. In the early days, important discoveries were made by qualitative interpretation of seismic-velocity anomalies mapped by the models. Since then, the seismic data sampling of the Earth has increased dramatically. Whereas the first global tomographic models were computed using hundreds of seismograms, the recent ones—using hundreds of thousands and millions of them. Is tomography's discovery potential reaching saturation? For qualitative interpretation of larger-scale features—yes, in many cases. For quantitative inferences—no, quite the opposite. The growth in the data sampling and progress in computational petrology and other relevant fields are now giving us a new ability: to resolve quantitatively what we want to know.

What to do?

1. **Thermodynamic inversion.** Computational petrology gives us the means to quantitatively relate temperature and composition at depth to elastic parameters (e.g., Connolly, 2005) and, then, to seismic observables (e.g., Fullea et al., 2012). This solves the forward problem. The corresponding inverse problem is non-linear. Posing and solving it for large datasets is an outstanding challenge. One approach for upper-mantle thermochemical imaging, for example, is to obtain a phase-velocity model for the region or the globe and, then, invert the Love and Rayleigh phase-velocity curves for temperature and composition, point by point (e.g., Fullea et al., 2021; Lebedev et al., 2023). The non-linear inverse problem for every column is small and can be solved readily and with exhaustive uncertainty analysis where needed.

2. **Seismic thermography.** Thermodynamic inversion can not only bring in extra, non-seismic information on what we want to know, but also help us to extract information from seismic data more fully and more accurately. A priori knowledge, such as the shapes of plausible lithospheric geotherms, reduces the non-uniqueness of the problem and steers the inversion to the physically plausible solutions within the broad misfit valleys in the model space. Because of the much greater sensitivity of seismic data to temperature than to composition, we can invert seismic data directly for temperature, with reasonable assumptions on composition and other relevant properties and with additional inversion parameters such as anisotropy. This amounts to Seismic Thermography of the Earth (Lebedev et al., 2024).

3. **A priori information.** The optimal resolution tomography of Bonadio et al. (2021) shows an example of an effective use of seismic *a priori* information—in this case, to solve the Backus-Gilbert problem (Backus & Gilbert, 1970) as applied to surface-wave tomography. We know that the phase-velocity curve at a point must be smooth, due to the inherent properties of the data. The roughness on the curves extracted from a set of phase-velocity maps thus gives us a direct estimate of the model error and a way to solve the Backus-Gilbert problem (finding an optimal resolving length at every point, defined as the narrowest one such that the model error at the point is under a threshold).

4. **Errors.** The largest uncertainty in 1D or 3D seismic-velocity models is normally due to parameter trade-offs. Covariance and resolution matrices can be computed, but they do not quantify directly the uncertainty of our inferences. Model-space projection (Bartzsch et al., 2011; Lebedev et al., 2013) can be easily applied to smaller inverse problems and

quantify the uncertainty of what we really want to know—for example, the lithospheric thickness or asthenospheric temperature.

JOINT INVERSION OF BODY AND SURFACE WAVES (Clifford Thurber)

Two end members of seismic tomography are body-wave arrival time tomography and full-waveform tomography. Arrival time tomography can be thought of as an infinite-frequency approach, whereas full-waveform tomography exploits a broad band of frequencies in fitting selected portions of seismograms. Lying somewhat in between these schemes are normal-mode and surface-wave tomography, that can again exploit broadband signals but which employ parametric inversions as used for arrival time work.

Arrival time tomography was developed in the mid 1970's in a series of papers by Keiiti Aki and coworkers on local and regional scale imaging (Aki & Lee, 1976; Aki et al., 1977) and has since been exploited in many different ways with a variety of inversion algorithms. Tomography exploiting normal modes and surface waves emerged in the mid 1980's in papers mainly by Adam Dziewoński and coworkers on global-scale tomography (Dziewonski, 1984; Woodhouse & Dziewoński, 1984; Dziewonski & Anderson, 1984). Over the past several decades, a variety of full-waveform tomography methods have been developed and applied to seismic imaging problems over a wide range of scales (Tromp, 2020), a notable example being SPECFEM3D (Komatitsch & Vilotte, 1998; Komatitsch & Tromp, 1999).

Full-waveform tomography is arguably the most powerful current approach to seismic imaging, but in practice its high computational demands tend to limit the model domain size, spatial resolution, and/or period range. An option for imaging with moderate resource demands is joint body-wave and surface-wave tomography (JBST), whereby both the arrival times of body wave phases and the dispersion characteristics of surface waves are jointly exploited. In this way, more of the content of seismograms can be utilised to constrain both P and S wavespeed distributions, and often a broader period range employed than is feasible with full-waveform inversion.

Two codes implementing JBST are by Fang et al. (2016), *jointTomoBS*, built on tomoDD (H. Zhang & Thurber, 2003) and by Eberhart-Phillips and Fry (2017), *simul2017*, built on simul2000 (Thurber & Eberhart-Phillips, 1999). The treatment of P waves is virtually the same in the two codes, but the way that S-wave and surface-wave data are used differs between the two methods, and also the calculation of sensitivities and the matrix inversion strategies differ. For Fang et al. (2016), S-wave arrival times and inter-station surface-wave group and/or phase travel times between station pairs over a range

of periods are used, and an approximate conjugate gradient method is employed for the matrix inversion. For Fang et al. (2016), residuals are simply the difference between an observed and the corresponding calculated inter-station group or phase travel time at a given period, and sensitivities for the matrix inversion are calculated somewhat analogously to body-wave sensitivities in terms of a wave path horizontally through the corresponding 2D group velocity map, with locally 1D sensitivity for each "column" of surrounding nodes vertically (Fig. 1). In contrast, Eberhart-Phillips and Fry (2017) use S-P times and 2D surface-wave group velocity maps for a range of periods, and a more accurate matrix inversion method (Cholesky decomposition) is used in conjunction with the hypocenter-velocity model parameter separation step (Pavlis & Booker, 1980; Spencer & Gubbins, 1980). In this case, residuals are evaluated between a group velocity value at a point in the 2D velocity map (yellow star in Fig. 2) and the predicted value based on a 1D average of velocities in a box centered on the selected point (red circles in Fig. 2). The width and depth extent of the box increases with increasing period. The sensitivities at all the points in the box are computed using the group velocity sensitivity kernels from the average 1D model for Vp and Vs, with Vs related to Vp and Vp/Vs.

Although these approaches to joint body-wave and surface-wave tomography are clearly a simplification and approximation compared to full waveform tomography, they have the advantages of combining the complementary sampling characteristics of Earth structure by body waves versus surface waves, the potential for finer-scale resolution with higher frequency data, and the method's computational efficiency.

One area for future work on further reducing the gap between such joint body-wave and surface-wave methods and full-waveform tomography is in improving the evaluation of sensitivities. The use of finite-frequency kernels (Marquering et al., 1999; Dahlen et al., 2000; L. Zhao et al., 2000; Tromp et al., 2005) for both body waves and surface waves appears to be the most logical target. The increased computational burden may be tractable with the use of adjoint methods. The computational tools for achieving this are generally available, including some recent "specialized" techniques. Among the latter are double-difference adjoint seismic tomography (Y. O. Yuan et al., 2016), sensitivity kernels for multicomponent ambient noise empirical Green's functions (K. Wang et al., 2019), and sensitivity kernels for differential travel time measurements using a three-station approach (X. Liu, 2020).

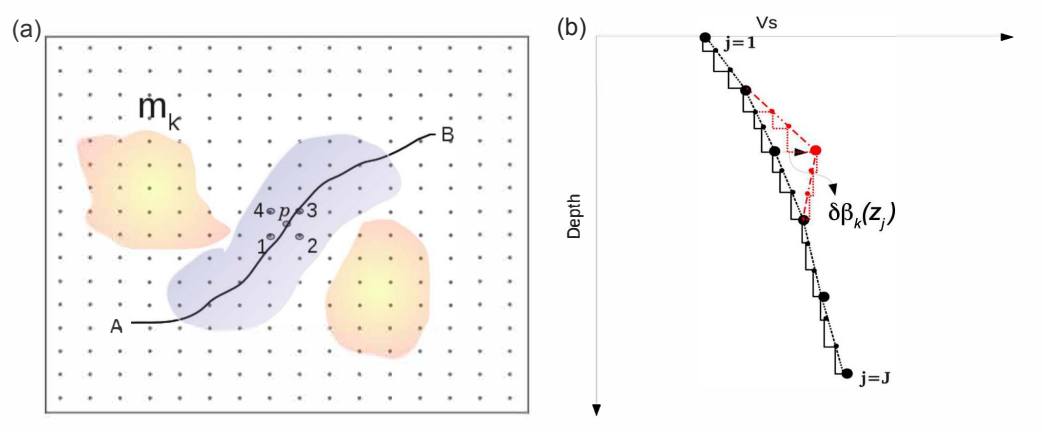


Figure 1. Illustration of the Fang et al. (2016) model discretization (a) Horizontal plane: The black solid line represents the propagation path between two stations A and B for the surface wave at some period. The phase slowness at any point p along the path is determined from the values at four surrounding horizontal grid points (1-4) using bilinear interpolation. (b) Vertical direction:The vertical grid model (bigger black dots with finer layers shown as the black line) is perturbed (as shown by the red dot and red dashed lines) to compute the depth sensitivity of dispersion data to model parameters via differences. Modified from Fang et al. (2016)

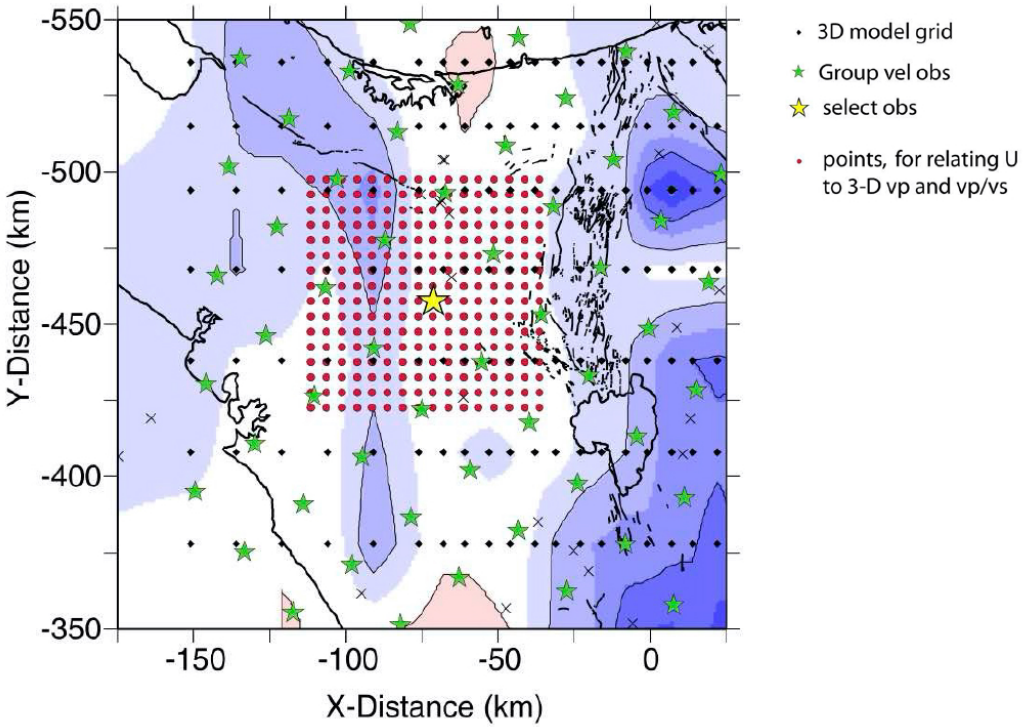


Figure 2. Map view of part of a velocity grid across New Zealand, showing an example of the box for computing group velocity (U) partial derivatives at points (red dots) in a volume surrounding a U observation (yellow star), analogous to points along a path from an earthquake travel time. Small dots are 3D velocity grid nodes; stars are U observation locations (nodes of U velocity map). From Eberhart-Phillips and Fry (2017).

SEISMIC TOMOGRAPHY AND INSIGHT INTO MANTLE PROPERTIES (Keith Priestley)

In seismic tomography research, there has always been the impulse to develop more accurate tomographic methods to eliminate simplifying approximations. For example, most tomography with surface waves employs the great-circle approximation (e.g., Woodhouse & Dziewoński, 1984; Ekström & Dziewonski, 1998; Lebedev & Nolet, 2003; Debayle & Ricard, 2012), even though this does not permit resolution of structures smaller than their sensitivity zone (e.g., Spetzler & Snieder, 2001; Yoshizawa & Kennett, 2002). Further improvement in resolution is being sought through utilizing more accurate forward calculations and adjoint tomography (e.g., Komatitsch & Tromp, 2002; Fichtner et al., 2006). While this is clearly the way forward, it is computationally intense, and at present, is limited in the number of seismic waveforms that can be inverted. The computational overhead will ease with future increases in computational power, but those increases will also require more efficient algorithms (e.g., Capdeville et al., 2002; van Herwaarden et al., 2020).

More complete subsurface tomographic imaging requires inverting waveforms whose various arrivals are sensitive to different parts of the Earth. To maximize the amount of information extracted from a waveform, a misfit function is required that permits retrieving information from low-amplitude phases in the presence of large amplitude phases, an active area of research, especially in the seismic exploration community (Virieux et al., 2017; Y. Yang & Engquist, 2018; Pladys et al., 2021).

Assessing uncertainties in seismic tomography models is a challenge because a formal resolution analysis is often not computationally feasible. In many cases, checkerboard tests are used with synthetic data that do not replicate the actual propagation paths nor are they faithful to the modal and frequency makeup of the observed waveforms. Lévêque et al. (1993) showed that checkerboard tests can be misleading, and that, contrary to generally accepted ideas, smaller-size structures can be well-retrieved while larger-size structures for the same data coverage are poorly retrieved. However, this issue is often ignored and more rigorous methods of quantifying model resolution are required.

Three key global-scale issues are the anisotropy, attenuation and viscosity of the Earth's mantle, and seismic tomography can make a major contribution in this area of research. Seismic anisotropy can be a key indicator of flow in the mantle. Models for 2Θ

azimuthal anisotropy from Rayleigh waves are converging, but there are few 4Θ azimuthal anisotropy measurements from Love waves. Radial anisotropy could potentially help to distinguish between horizontal and vertical flow in the mantle. However, existing models of radial anisotropy, while showing general agreement on scales of thousands of kilometers, display little agreement for smaller-scale features. Extracting 4Θ azimuthal anisotropy and radial anisotropy depends on the analysis of horizontal-component data, which almost always contains higher noise than vertical-component data. Some studies have exaggerated the radial anisotropy problem by using Love and Rayleigh wave results from different sources, causing non-uniform path coverage. In addition, where radial anisotropic models are derived purely from fundamental-mode data, additional issues arise because, for a given period, Rayleigh and Love waves sample the subsurface differently.

S wavespeed models for the mantle show good agreement, but mantle attenuation models differ significantly in terms of both the geometry and magnitude of the variations. Such problems are not surprising, since it is more difficult to measure variations in the amplitude of a seismic wave than it is to determine its arrival time. It is not even straightforward to calculate the amplitude variations for a particular model because lateral velocity variations lead to amplitude variations due to focusing and defocusing. Despite such problems, all authors who have studied mantle attenuation have remarked that attenuation and shear wave speed are generally correlated.

Estimates of the 3-D thermal structure of the upper mantle have been deduced from seismic tomography (e.g., McKenzie et al., 2005; Priestley & McKenzie, 2006; Cammarano et al., 2011; Priestley & McKenzie, 2013) and so achieved reasonable resolution. However, 3-D viscosity structure remains poorly resolved, despite being an important factor in mantle convection patterns (e.g., Bunge & Richards, 1996) and in controls on the evolution of sea level. Recent observations from Antarctica, where strong upper mantle contrasts in viscosity likely exist, show that ignoring 3-D variations in viscosity can lead to significant errors in understanding the GPS uplift rate, water/ice mass balance and sensitivity to changes in ice thickness (e.g., van der Wal et al., 2015; Powell et al., 2020). Therefore, many applications that require a 3-D viscosity model have derived it from seismic tomographic images (e.g., Lau et al., 2018). Such conversions are largely based on empirical choices of scaling relationships between seismic wavespeed and viscosity (e.g., Austermann et al., 2013), but recent work has combined seismic tomogra-

phy results with laboratory results to derive a "less" *ad hoc* relationship between seismic wave speed and viscosity (e.g., Priestley & McKenzie, 2013; Priestley et al., 2024).

MULTI-PARAMETER INVERSION: ALL OR NOTHING!? (Andreas Fichtner

Tomographic inversions for isotropic P and S wave speeds have long been a standard because reliably measurable body wave arrival times and surface wave dispersion are primarily sensitive to these parameters. Parameters with mostly smaller sensitivity, including anisotropy, attenuation and density, continue to be comparatively weakly constrained, despite their fundamental role in studies of temperature, composition and flow inside the Earth. While it would be desirable to constrain these parameters all at once, practical inversions limit the number of parameters to not more than a handful. In addition to computational cost, the fundamental reasons are (i) the increasing impact of subjective regularization choices as sensitivity decreases, and (ii) our inability to independently constrain a large number of parameters with the available data.

The difficulty of multi-parameter inversion can be explained mathematically with the help of Newton's method (e.g., Kennett & Sambridge, 1998). Though not often used in practice, it allows us, in principle, to constrain a vector $\mathbf{m}$ with components m_i representing the distributions of wave speeds, up to 21 elastic tensor components, attenuation, etc. Denoting by $\mathbf{g}$ and $\mathbf{H}$ the gradient and the Hessian of the misfit functional χ, Newton's method yields the model update $\delta\mathbf{m} = -\mathbf{H}^{-1}\mathbf{g}$. If all parameters were uncorrelated, the resulting diagonal Hessian would allow us to consider each parameter individually via $\delta m_i = H_{ii}^{-1} g_i$. Any parameter m_i could either be included or dropped at will without affecting inferences of other parameters $m_{j\neq i}$. In reality, parameters are correlated, and the update is given by

$$\delta m_i = H_{ii}^{-1} g_i + \sum_{n\neq i} H_{in}^{-1} g_n \ . \tag{1}$$

Other optimization algorithms, and quasi-Newton methods in particular, effectively produce Eq. (1) through iterative updating (Nocedal & Wright, 1999). Eq. (1) contains an obvious contradiction to item (ii) above. When significant trade-offs between parameters, described by the off-diagonal elements of $\mathbf{H}^{-1}$, are expected, these parameters can actually not be dropped. However, when trade-offs are small, the corresponding parameters may just as well be included. Furthermore, Eq. (1) demonstrates that, in contrast to common practice, the choice to include a parameter m_i cannot be based solely on the size of its sensitvity g_i. Instead, knowledge about the cumulative trade-offs with all other parameters, $\sum_{n\neq i} H_{in}^{-1} g_n$, is required. In this sense, we may be in the fortunate situa-

tion that a parameter with small sensitivity is comparatively well constrained because the cumulative trade-offs with other parameters are small. Conversely, a parameter with large sensitivity may be difficult to resolve when trade-offs with seemingly unimportant parameters have a large cumulative effect.

While second-order adjoint techniques (Santosa & Symes, 1988; Fichtner & Trampert, 2011) provide efficient access to individual Hessian-vector products, the computation of $\sum_{n \neq i} H_{in}^{-1} g_n$ for a large number of parameters is computationally demanding. We therefore lack an easy criterion to inform us about the parameters that should be included or may be dropped.

The most profound consequence is that we cannot proceed incrementally, because we do not know which the next meaningful increment should be. Including some of many parameters that describe anisotropy may be as (un)justified as including a parameter for attenuation, because the cumulative trade-offs with all other parameters are unknown. Experimental design approaches, either at the level of model parameters (Sieminski et al., 2009) or misfit functionals (Bernauer et al., 2014) may help to suppress parts of $\sum_{n \neq i} H_{in}^{-1} g_n$, but still require information on $\mathbf{H}^{-1}$ to check if this goal has actually been achieved. In the absence of a quantitative ordering, we may be forced to include all parameters in order to avoid artifacts caused by insufficiently informed decisions concerning their relative importance. This closes the circle to the regularization and trade-off problems (i) and (ii), explained above.

Both problems can, in principle, be avoided by regularization-free Bayesian inference methods. Practical implementations of Bayesian inference, for instance, in the form of Hamiltonian Monte Carlo (Fichtner et al., 2019) or variational inference (X. Zhang et al., 2022) allow us to consider higher-dimensional model spaces, relevant for seismic tomography, but will require further improvements to solve large multi-parameter problems. The design of meaningful priors that go beyond the standard Gaussian or constant distributions through the incorporation of petrological and geostatistical information will be instrumental in making multi-parameter Bayesian inference efficient and practical.

UNCERTAINTY IN SEISMIC TOMOGRAPHY (Nick Rawlinson)

When presented with a "final model" produced by seismic tomography, which might contain coherent anomalies that appear ripe for interpretation, the first question one should always ask is "what can I believe"? This is an excellent question, because the inverse problem that lies at the heart of seismic tomography is ill-posed, with multiple models capable of satisfying the data. Of course, you might be tempted to say "wait, if I parameterise my model with one single constant velocity block, then the solution must be unique!". This fails on two levels: first, you have arbitrarily selected your parameterization, and an infinite variety of other options also exist that are equally (or probably more!) justifiable; second, you are unlikely to fit the data with a single parameter, and even if you can, the presence of data noise precludes there being a unique solution. As noted by Keiiti Aki in his seminal paper (Aki et al., 1977) the ideal parameterization might ostensibly be one that has a scale length on par with the seismic wavelength. However, the data coverage will almost never be sufficient to make this a worthwhile endeavour. Irregular parameterizations, where one attempts to vary the spatial scale-length of the underlying parametrization (e.g. by employing an unstructured mesh) to somehow match the data coverage is a balancing act of trying to make the inverse problem as well-posed as possible, while at the same time maximising the extraction of information from the dataset (Bijwaard et al., 1998; Fang et al., 2019).

In addition to data noise and parametrization choice, there are other factors that contribute to model uncertainty. Typically one makes assumptions about anisotropy, since inverting for all 21 independent elastic moduli is generally out of the question; as a result, unmodelled anisotropy will manifest as model uncertainty in a way that is difficult to quantify. Assumptions in solving the forward problem will also play a role in model uncertainty – for instance, the use of ray theory to predict traveltimes is a well known approximation that gets poorer as the ratio between seismic wavelength and structural wavelength increases. Unsurprisingly, the above issues are well recognised by the seismology community, and they have not been idle in seeking out novel approaches for addressing such challenges.

With ongoing increases in computing power, inversion methods that produce an ensemble of data-satisfying models rather than a single model are becoming more popular (X. Zhang & Curtis, 2020; Fichtner et al., 2019). The advantage of this approach is that the ensemble can be interrogated for common features that are required by the

data. An approach known as transdimensional (transD) tomography (Bodin & Sambridge, 2009; Bodin et al., 2012), which employs a reversible jump Markov chain Monte Carlo (rj-McMC) scheme to construct a posterior probability density function (PDF) from a prior PDF and likelihood function within a Bayesian framework, has become quite popular in recent years. It allows for the number of unknowns in the inverse problem to also be an unknown, and through an hierarchical approach, can include noise parameters in the inversion. Typical models are built on unstructured or nested parametrizations that are amenable to redistribution, densification and removal in an effort to extract the maximum information from the data with the fewest parameters. The posterior PDF is typically distilled by taking the mean (or median) model as the "final" model, and the standard deviation as a measure of uncertainty. This approach is less valid if the posterior PDF does not have a unimodal distribution. Despite the data driven nature of transD, like other tomography methods, it still depends on the quality of prior model information and data uncertainty estimates, which are often poor. As a consequence, it is not immune from the need to make ad hoc decisions in order to produce what can be regarded as "reasonable" results.

As new methods continue to be developed and computing power increases, our ability to account for solution non-uniqueness in seismic tomography will continue to improve. Perhaps the most challenging issue to deal with is data noise, since invariably it is poorly constrained, and even the distribution is generally not well understood. Most misfit or objective functions employ an L_2 measure of misfit, which is optimal if the noise has a Gaussian distribution, but otherwise is not robust to outliers, something that is difficult to guard against without removing potentially important data. Aside from methodological improvements, the use of increasingly large volumes of data that include considerable redundancy is another important way forwards. This can be seen in regional or global traveltime tomography for example, where individual measurements may carry substantial picking error, but huge numbers of nearby earthquakes can be exploited to clean up signal (eg. by clustering and stacking), which is essential for producing good models (Zenonos et al., 2019). In exploration, excellent coverage of (usually) high quality data with inherent redundancy, coupled with good prior information, is largely responsible for the active source version of FWI (Full Waveform Inversion) becoming a standard technique that can retrieve remarkably detailed and well-constrained images of the subsurface (Mancini et al., 2016).

RESOLUTION OF (AN)ELASTIC MANTLE MODELS (Ebru Bozdağ)

Efficient numerical wave propagation solvers and high-performance computing have opened new frontiers in passive-source seismic tomography by taking the full complexity of wave propagation into account in the inverse problem (e.g., C. Tape et al., 2009; Fichtner et al., 2009; French & Romanowicz, 2015; Bozdağ et al., 2016; Lei et al., 2020). Yet, it is challenging to "peel off" the outer heterogeneous layers of the Earth to image the target depths of interest where the complex physics of the medium and the seismic source must similarly be addressed in inversions. The ideal is to update all seismic parameters simultaneously (i.e., wavespeeds, density, anisotropy, anelasticity, and source parameters). However, the trade-off between parameters exacerbated by the uneven distribution of seismic sources and receivers concentrated at the surface makes such comprehensive inversion challenging.

Although full waveforms are computed numerically, the first-generation adjoint tomography models in earthquake seismology were built using phase measurements only. This choice was made to minimize the trade-off between model parameters by targeting the elastic properties of the media. Amplitudes of seismic phases are sensitive to the nonlinear combination of scattering/defocusing, anelasticity, source radiation pattern, and scalar moment (e.g., Dalton et al., 2008). Yet, if they can be assimilated properly, amplitudes can provide unique constraints to locate heterogeneities (e.g., Laske & Masters, 1996) as they are sensitive to the gradient of phase speeds (Woodhouse & Wong, 1986). However, one needs to address the anelasticity and source parameters with the elastic structure, specifically at the global scale.

Attenuation (Q^{-1}, inverse of quality factor Q) models are important not only for constraining the water content, partial melting, and temperature variations in the mantle (e.g., Anderson, 1967; Karato & Jung, 1998) but also for the character of elastic models. It is generally assumed that a suitable radially symmetric Q^{-1} model can capture the physical dispersion of seismic waves (e.g., Kanamori & Anderson, 1977). However, there is no consensus even on the 1D Q structure (e.g., Resovsky & Trampert, 2002). This leads to two major consequences for elastic models:

1. Wavespeeds of elastic models involve physical dispersion from the Q^{-1} models used in their inversion, which is often significant and needs to be corrected before any model comparisons.

2. Since elastic models are constructed as perturbations around chosen Q^{-1} models, any uncertainty in Q^{-1} may be mapped onto elastic models.

Figure 3 shows a simple comparison of minor- and major-arc Rayleigh waveforms computed for the same elastic model, GLAD-M25 (Lei et al., 2020), but with different Q^{-1} models in the upper mantle; QL6 of (Durek & Ekström, 1996) and QM1 of (Widmer et al., 1991). The waveforms are filtered between 40-250 s, a typical period band for surface-wave data in global tomographic studies. For this example, Q^{-1} models cause ~ 22 s time shift on the major-arc Rayleigh wave, which is more than half a cycle of the minimum period of the waveforms. The effect of the different Q^{-1} models is less on body waves but still can be significant relative to their measured time shifts. Therefore, it is essential to perform full-waveform inversions by simultaneously updating Q^{-1} and elastic models, not only to construct Q^{-1} models to provide additional constraints on the mantle's thermo-chemical structure but also to continue to improve the elastic models.

However, in practice, it is challenging, if not impossible, to independently retrieve elastic and anelastic models due to uncertainties in the nature of the medium (i.e., anisotropy) and source parameters. One recommended approach is the sequential inversion of elastic and anelastic parameters, which allows mitigation of the trade-off at each iteration (e.g., Karaoğlu & Romanowicz, 2018). Designing appropriate measurements to be used for full-waveform inversions, such as those based on amplitude ratios of different phases (e.g., Ritsema et al., 2002) or double-difference phase misfits (Y. O. Yuan et al., 2016), may help reduce source uncertainties. Still, the problem of fully characterizing the anelastic Earth is complex due to the trade-offs between seismic parameters, and better resolution can only be achieved by updating elastic and anelastic parameters simultaneously or sequentially. This issue highlights the importance of uncertainty quantification in tomographic models. Meanwhile, the problem of adequate resolution is naturally worsened by the uneven global data coverage – where we need more data, specifically from oceans. Emerging technologies such as DAS, nodal arrays, etc. provide unprecedented sampling of the continents and offshore, complementing dense broadband arrays. MERMAIDs (e.g., Simons et al., 2021) are promising to efficiently sample the oceans by acoustic means while we ultimately would like to see USArray-type ocean-bottom seismometer arrays. All these new opportunities need to be carefully analyzed and integrated into seismic tomography to maximize the benefit of emerging instruments and big data in seismology.

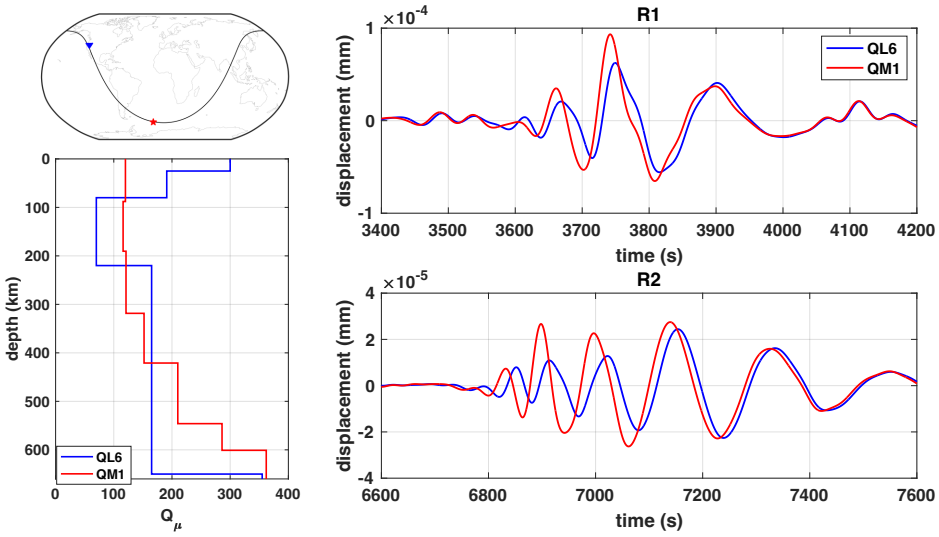


Figure 3. Effect of upper-mantle attenuation on vertical-component minor- and major-arc Rayleigh waves (right panel) where the corresponding ray paths are shown top left. Simulations are performed for the 3D mantle model GLAD-M25 (Lei et al., 2020) with 1D Q model QL6 (Durek & Ekström, 1996) (blue) and with QM1 (Widmer et al., 1991) in the upper mantle (red) as shown bottom left. Seismograms were computed by the 3D global wave propagation solver SPECFEM3D_GLOBE (Komatitsch & Tromp, 2002) and filtered between 40-250 s. Figure courtesy Rıdvan Örsvuran.

WHAT ARE TOMOGRAPHY'S LIMITATIONS? (Jeroen Ritsema)

For many end users, tomography is a black box that magically turns seismic data into tantalizing pictures of Earth's interior. Convenient tools like SubMachine (Hosseini et al., 2018) help scientists explore the images and reconcile velocity anomalies with other geophysical observations. It is fair for seismologists to present tomography as an important technique for mapping Earth's composition but they must expose tomography's observational constraints, modeling choices, and other secrets. Image resolution is heterogeneous and uncertainties are uncertain – no matter which tomographic model is one's favorite.

Even the biggest structures in tomographic maps are not fully understood. A case in point is the nature of the large-low velocity provinces (LLVPs) that may play a key role in global mantle circulation (e.g., McNamara, 2019). "Vote maps" of Vs models agree on the LLVPs' areal extent (Cottaar & Lekic, 2016), but mineral physicists want Vs and Vp and geodynamicists want density. The Vp structure at the core mantle boundary is poorly resolved because diffracted P waves have a short reach, PcP signals are weak, and no seismometer on Earth has recorded a PKP wave through LLVPs. The traveltimes of P waves from earthquakes in the Tonga region to seismometers in North America form the bulk of the P wave constraints on the Pacific LLVP. In eastern North America, these P waves are recorded with a delay of less than a 1 second whereas the average S wave delay is 5 seconds. "Reasonable" estimates of the Vs and Vp structure can explain these traveltimes delays (Figure 4) but the $\mathrm{dln}V_S/\mathrm{dln}V_P$ ratio of the LLVP, important for differentiating thermal and chemical origins of seismic heterogeneity (e.g., Karato & Karki, 2001), depends on the resolution of Vp of the North American lithosphere. Constraints on the LLVP's density depend on Vp and other factors (Robson et al., 2022). It remains uncertain whether LLVPs are relatively dense or light.

It is natural that tomography takes advantage of super computers and "big data" approaches. The use of fuller waveforms with higher frequency content will enhance image resolution on global (e.g., French & Romanowicz, 2014; Lei et al., 2020), regional (e.g., Cupillard et al., 2012), local (e.g., C. Tape et al., 2010), and multi scales (e.g., Fichtner et al., 2018). Deployments in the oceans, (e.g., Suetsugu & Shiobara, 2014; Tsekhmistrenko et al., 2021; Pipatprathanporn & Simons, 2022) and in countries such as China (S. Yuan & Xu, 2019), Brazil (Bianchi et al., 2018) and on the African continent (Nyblade et al.,

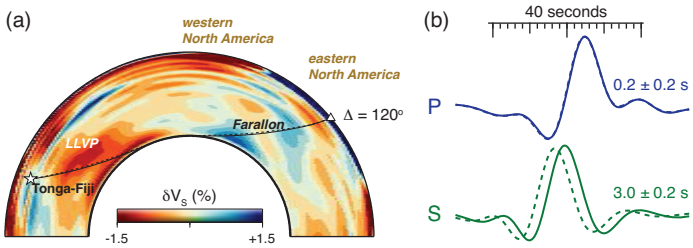


Figure 4. (a) The degree-12 Vs structure S12 – similar to other global-scale tomographic Vs models for the mantle (e.g., Ritsema & Lekić, 2020) – along a great circle through the southwestern Pacific region on the left and North America on the right. The star indicates the hypocenter of an earthquake beneath Tonga-Fiji. The triangle is at an epicentral distances of 120°. (b) Spectral-element-method (Komatitsch & Tromp, 1999) waveforms of the P and SH wave for a distance of 120°, computed for (dashed lines) PREM (Dziewoński & Anderson, 1981) and (solid lines) S12 and P12. P12 differs from S12 by a scaling factor R that increases from 1 in the upper mantle to 3 in the lower mantle, consistent with global travel time measurements (e.g., Robertson & Woodhouse, 1996; Ritsema & van Heijst, 2002). The numbers on the right indicate the misalignment between the S12/P12 and PREM signals. The P wave's deceleration in the LLVP and its acceleration in the *Farallon anomaly* and the lithosphere of eastern North America are equal so the P-wave arrival time is the same as the PREM predicted arrival time. This figure is a modification of Figure 9 in Chaves et al. (2020).

2011) where global network coverage is relatively low, are essential to diversify wave coverage. New techniques for the modeling of body wave triplications (Staehler et al., 2012), and wave conversions (de Jong et al., 2022) and reflections (Z. Guo & Zhou, 2019) at the '410' and '660' km discontinuities may help to improve the relatively poor resolution in the transition zone, a layer known to impede convective flow.

It is also important to collaborate with the users of tomography to ensure that our geophysical research questions are in sync and to optimize tomography as the best tool for the testing of hypotheses of deep-Earth physics. Image visualization must be accompanied with practical tools for interrogating image resolution. Mapping Earth's structure with finer detail remains a worthwhile effort but *how does Earth work?* is not a question for tomographers alone.

PRESENTATION AND COMPARISON OF TOMOGRAPHIC MODELS (Brian Kennett)

Many decisions have to be made in setting up a tomographic model, and some, such as the choice of the position of discontinuities can have significant effect on the actual outcome. Such effects are noticeable in global models because of the influence of the major discontinuities in the mantle transition zone. There is a tendency for apparent heterogeneity to increase in the neighbourhood of assumed discontinuities, which may be real but can arise from misplacement of interfaces. The presence of strong discontinuities in the base model employed without direct correspondence in the data can lead to notable distortions in the extracted results. For example, the very strong 210 km discontinuity in PREM (Dziewoński & Anderson, 1981) produces distinctive effects in inversions that are not present when no discontinuity is introduced (Kustowski et al., 2008).

Another class of prior assumptions that can have significant effects on the outcome relate to the continuity of heterogeneity structure. In global models, a common choice is to allow different styles of behaviour above and below the "660 km" discontinuity to separate upper and lower mantle, as for example in the model GLADM-25 (Lei et al., 2020) obtained with full-waveform inversion. However, the mantle transition zone extends further in depth with garnet phases only eliminated at about 800 km, so this choice is more arbitrary than it seems. There is strong evidence for significant viscosity contrast between the uppermost mantle and the deeper parts, but the depth of the end of the viscosity increase is not well constrained. Placing a discrete boundary for heterogeneity coincident with the wavespeed jump is a specific assumption.

As knowledge of 3-D structures has grown it is less common for tomographic results to be obtained by a single-pass linearized inversion from a reference model. But still most models are created, and stored, as a set of perturbations from some reference. In the case of inversions based purely on relative travel times it is not entirely clear what this reference may be. Where possible, the inclusion of absolute timing can help resolve such issues. Inter-comparison of 3-D models is facilitated by presenting results in terms of absolute velocities. This approach also has the merit that any impact from an underlying reference model is fully represented.

Many tomographic results are plotted as perturbations from radial reference models that have been chosen for convenience or constructed in association with the 3-D model,

such as model GAP_P4 (Obayashi et al., 2013), and the radial profile for GLADM-25 (Lei et al., 2020). Such a procedure may appear a natural consequence of model construction, but can obscure the impact of specific assumptions or features in the underlying model. Authors should be encouraged to present their plots relative to well-known reference models. Suitable comparator models should have relatively bland properties, with the minimal presence of discontinuities. In this way direct visual and numerical comparison between different styles of models is facilitated. For long-period work, STW105 (Kustowski et al., 2008) is a good choice as a reference since it retains the lower mantle character of PREM without as much shallow complexity. For higher-frequency work, ak135 (Kennett et al., 1995) has proved quite effective for a wide range of both P and S studies.

It is important to exploit the full available control on the physical properties of the Earth, especially where comparisons are to be made with mineral physics predictions. In this context comparison of wavespeed models from different wavetypes with differing resolution can lead to potentially misleading conclusions. For the full mantle S coverage is more readily secured than for P, but in regional studies P readings are likely to be much more plentiful than for S, as in the work of D. Zhao et al. (2021).

For travel-time tomography comparable coverage can be achieved by choice of only paths for which both P and S have been picked (Kennett et al., 1998; Gorbatov & Kennett, 2003). This approach only provides a quality control filter on the data, but also means that wavespeed ratios are meaningful. In these circumstances it useful to look at joint tomography to extract bulk-sound speed as well as P and S properties (Kennett et al., 1998). For full waveform inversion, good P wave coverage to supplement S can be achieved if appropriate windows of seismograms are exploited, though the generally smaller amplitudes of P phases can mean reduced sensitivity.

Ideally comparisons of images for different wavetypes should be made with comparable wavelength for P and S sampling. Except in areas of high attenuation, the frequencies of S arrivals for teleseisms are roughly half those for P. Thus, P and S wavelengths are similar. For waveform inversion, the maximum frequency employed is likely to be dictated by computational considerations, but selective filtering can help with equalisation.

FULL WAVEFORM INVERSION FOR GLOBAL MANTLE STRUCTURE, WHAT'S NEXT: (Barbara Romanowicz)

A fundamental requirement for successful tomographic imaging is the appropriate illumination of the target region, requiring each sub-volume to be sampled by waves propagating in different directions. This requirement is even more severe when the structure sampled is seismically anisotropic. As well-meaning mathematicians have shown (e.g. Castelvecchi, 2017), if the Earth's surface were densely and uniformly covered by both sources and receivers, we could uniquely resolve the seismic structure of the mantle - at least its isotropic part -using only P and S travel times. In practice, such a proposition is unrealistic. So, in order to compensate for the uneven and often sparse distribution of earthquake sources and stations, more information needs to be extracted from each seismogram. This is where the power of full waveform inversion (FWI) lies: it makes it possible to exploit the information contained in every wiggle of a seismogram, produced by all the different seismic waves that bounce and scatter inside the Earth, whether or not they can be easily separated on the record.

FWI requires the computation of the complete seismic wavefield in a 3D Earth. While early global FWI models were based on normal mode perturbation theory (Woodhouse & Dziewoński, 1984; Li & Romanowicz, 1996; Mégnin & Romanowicz, 2000), a major step forward was the introduction to global seismology of an efficient method to solve the wave equation numerically, the Spectral Element Method (SEM) (Komatitsch & Vilotte, 1998; Komatitsch & Tromp, 1999)), which lifted restrictions on the smoothness and wavelength of the 3D structure, at the expense of increasing computation time, which grows as the fourth power of frequency. Importantly, it made it possible to compute accurate misfit surfaces. This led to first generation global mantle models that compute the forward wavefield accurately using SEM (Lekić & Romanowicz, 2011; French & Romanowicz, 2014; Bozdağ et al., 2016; Lei et al., 2020), but differ in their inversion methodologies, and in particular in the way sensitivity kernels are computed. A comparison and discussion of the pros and cons of the different choices made for data processing and inversion used in these two approaches is presented in Romanowicz (2023).

In addition to exploiting the main phases bouncing between the surface and the core-mantle boundary, FWI based on the SEM (or other accurate numerical methods for wavefield computation) has the potential of exploiting information in the coda of the main seismic phases, which is particularly important for resolving low velocity regions

of small dimensions, hidden from view in conventional travel time measurements by the phenomenon of wavefront healing (e.g. Nolet & Dahlen, 2000). This is already apparent in the emerging resolution of deep mantle plumes in the latest SEM-based models (e.g. French & Romanowicz, 2015; Lei et al., 2020).

Going forward, one possible way to improve resolution in FWI is to work towards reaching higher frequencies, which comes at great computational expense. However, illumination becomes a problem again. While it is essential to keep maintaining the high quality international global very broadband seismic network, and complementing it by regional continental and especially seafloor deployments, including efforts such as MERMAIDS (Sukhovich et al., 2015), achieving high resolution uniformly at the global scale is not a realistic goal. Promising approaches are using adaptive grids that can be refined in well-illuminated regions (e.g. Thrastarson et al., 2020), or, alternatively, aiming to resolve well-illuminated regions of geophysical interest, possibly complemented by targeted, long duration, broadband instrument deployments. For targets in the deep mantle, far away from sources and stations (for example roots of mantle plumes), such an approach would still require heavy computations if the entire wavefield is recomputed at each iteration. Here, a particularly promising methodology is "Box Tomography", in which the wavefield computations are broken into three parts: (1) from the source to the boundary of the target region, (2) within the target region, and (3) from its boundary to the recording stations. The long distance wavefields in (1) and (2) are computed only once in the best possible, relatively smooth, background model, while model iterations are performed only within the box (Figure 5). This separation can significantly reduce computational time, and the illumination requirement needs only be verified within the target region. Concerns have been raised about mapping unmodeled outside heterogeneity into the box. However, with robust illumination by crossing paths within the box, such outside structure affects only a specific swath of paths and will be incompatible with measurements on paths from other directions, which will prevent its projection into the box. Masson and Romanowicz (2017) illustrated the power of such an approach (albeit in 2D) by showing how the structure in a box located at the CMB can be recovered even if the background mantle model is assumed to be 1D. Such box methodology is under development using existing SEM-based computational tools (e.g. Leng et al., 2020; Pienkowska et al., 2021; Adourian et al., 2021). In the future, it should be able to take advantage of novel, more efficient solvers (e.g. Masson, 2023) and may eventually lend itself, within

relatively small target regions, to full waveform Bayesian inversion in 3D, or other AI methodologies.

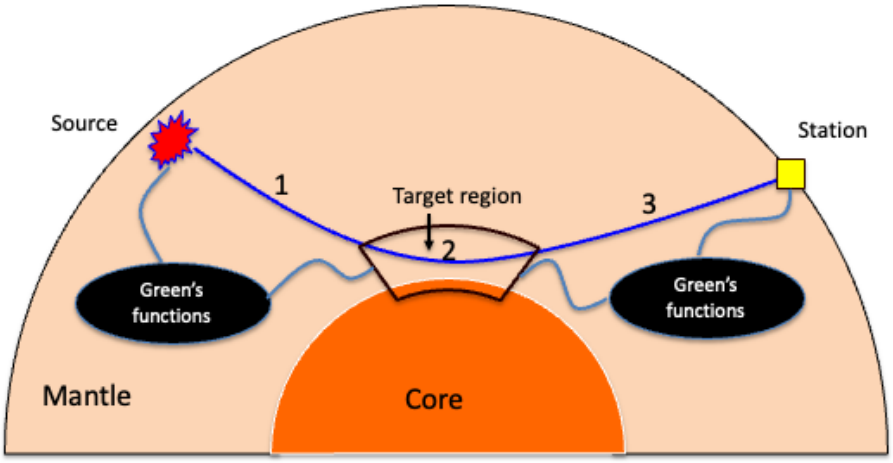


Figure 5. Box Tomography set up for imaging of a remote target region in the Earth. The Green's functions (1) and (3) are pre-computed in a reference global model and recorded at the boundaries of the target region. FWI proceeds with wavefield computations restricted to the target region (2). Time reversal mirrors allow the reconstruction of the full wavefield from the remote source to the remote station, at each iteration.

ADJOINT WAVEFORM TOMOGRAPHY FOR NEXT-GENERATION SEISMIC ANALYSES AND MONITORING (Arthur Rodgers)

The development of methods and capabilities to compute complete waveform simulations in three-dimensional (3-D) Earth models along with adjoint methods for computing the fully 3-D sensitivity kernels in the 2000's (e.g., Tromp et al., 2005; Fichtner et al., 2006) set the stage for new advances in seismic imaging (Tromp, 2020). In my opinion the full benefits of adjoint waveform tomography (AWT) are not yet fully realized, and this will be an important direction for the future of seismic tomography.

Full-waveform inversion has the advantage of fitting the data we actually record on seismometers rather than derived observables, and perhaps more importantly it includes the full finite frequency sensitivity to 3-D structure. The framework of AWT includes the necessary physical material properties needed to simulate waveforms in 3-D (i.e., shear and compressional wavespeeds, anisotropy, density, attenuation, discontinuities) although not all may be solved for. However, full-waveform inversion comes with challenges; most importantly it is both data and computationally intensive. Large data sets (many events and receivers) are needed to provide azimuthally distributed and redundant geographic sampling to triangulate anomalies. Many iterations are needed to converge inversions of longer to shorter period waveforms through a conservative multiscale approach. The main challenges are the computational effort needed to compute forward and adjoint simulations for many events and many iterations, and the processing of all waveform windows and misfits. Recent advances in AWT workflow efficiency, implemented in dedicated software packages such as the Large-Scale Seismic Inversion Framework (LASIF) (Krischer et al., 2015; Thrastarson et al., 2021), SeisFlows (Modrak et al., 2018), Pyatoa (Chow et al., 2020) or Salvus (Afanasiev et al., 2019) and high performance computing (HPC) platforms, e.g., hybrid central and graphics computing unit acceleration, large shared memory nodes, are making it possible to run more iterations on larger data sets more quickly than was previously possible. It is important not to forget that waveform inversion can also suffer from the problems that plague all seismic tomographic inversions (e.g., data coverage, uncertainties in source parameters, model parameterization and regularization). However, the fully 3-D sensitivity of the complete waveform to structure enables AWT to use scattered arrivals and constrain larger volumes of the Earth compared to traditional methods (e.g. ray theory, path-average approximation). Rodgers et al. (2022) ran a multiscale AWT inversion for the western United

States and used about ten times more iterations compared to previous studies. The resulting WUS256 model provided greatly improved waveform fits over previous models based on AWT and surface wave dispersion tomography.

The promise of AWT is to provide 3-D models that can reliably simulate observed waveforms. Current research must focus on evaluation of the validity of 3-D seismic models obtained with AWT, including investigations of how models perform for other seismic observables (e.g., body wave travel times and surface wave dispersion). This community must discover and understand the limitations of AWT to achieve good waveform fits at shorter periods resolving finer-scale structure. That is: what kinds of waveform data and measurements are needed to improve the coverage? How can validation and resolution be reliably assessed? How can computational resources be most efficiently used, especially as the effort of simulations increases as frequency to the fourth power?

The benefits of 3-D Earth models fitting shorter periods are manifold not only for geologic/tectonic interpretation of structure but for immediate societal applications such as seismic hazard and operational earthquake and explosion monitoring. One important target would be to image the upper crust in areas of high seismic risk on sub-kilometer scales for earthquake strong motion simulation and analysis (frequencies of $\sim$1 Hz or higher). Another use-case would be regional-scale source characterization (location, depth, moment tensor) with full waveforms for seismic hazard, reservoir and mine seismicity as well as sparse network global explosion monitoring (e.g. the Comprehensive Nuclear Test Ban Treaty International Monitoring System).

If AWT models prove successful at reproducing independent waveform observations they will be useful for these and other analyses. Green's functions for proven models could be pre-computed on HPC using reciprocity for a fixed network of stations and made available via web or cloud services. Although the storage requirements for regional-scale Green's function databases are tremendous, this would make synthetic seismograms for 3-D models available for immediate (e.g., operational pipeline) use without the need to run arduous event-specific HPC simulations. Furthermore, such stored seismograms enable probabilistic (stochastic) forward and inverse calculations of ground motion intensity or source properties. The benefits and use-cases for improved waveform-based 3-D seismic Earth models await for the seismic tomography community to fully realize the advances that were previewed in Toronto and are highlighted in this special issue.

ADVANCING WAVEFORM INVERSION BASED ON SOURCE ENCODING AND MODEL-ORDER REDUCTION (Jeroen Tromp)

Thanks to modern numerical methods and high-performance computers, seismic full waveform inversion (FWI) has been fully realized, as envisioned by Bamberger et al. (1977), Lailly (1983), and Tarantola (1984). FWI is now used across nine orders of frequency and wavelength, from megahertz frequencies and millimeter wavelengths in ultrasound medical imaging and nondestructive testing to millihertz frequencies and thousand-kilometer wavelengths in earthquake seismology. The ultimate goal of FWI is to use every wiggle in a seismogram to understand the Earth's physics and chemistry.

Full-waveform inversion is continually being developed and improved, with the potential for a more complete description of the physics of seismic wave propagation and better optimization algorithms. Numerous reviews, such as those by Virieux and Operto (2009); Fichtner (2010); Q. Liu and Gu (2012); Tromp (2020), provide further insight into the advancements of FWI.

In this section, I will provide a brief overview of three promising methods: source encoding, model-order reduction, and Hamiltonian Monte Carlo (HMC). Combining model-order reduction with source encoding can lead to a significant shift from using iterative quasi-Newton local optimization methods to HMC global optimization methods. This shift enables faster and high-resolution imaging while also allowing for uncertainty quantification. Speed is crucial for time-sensitive imaging, such as mammography. Additionally, the interpretation of FWI tomographic images requires accurate quantifiation of uncertainties to assess the thermochemical origin of wavespeed variations in the Earth's deep interior.

Source encoding: In traditional time-domain FWI, an inversion is independent of the number of receivers but scales linearly with the number of sources. To ameliorate this problem, exploration seismologists developed Source Encoding (Krebs et al., 2009; Ben-Hadj-Ali et al., 2009; Choi & Alkhalifah, 2011; Schuster et al., 2011; Schiemenz & Igel, 2013; C. Castellanos et al., 2015; Z. Zhao et al., 2016), where data from different sources are combined in one encoded 'supergather'. The challenge had been that the encoded contributions from distinct sources are difficult to completely unravel, leading to 'crosstalk' (Romero et al., 2000), which contaminates Fréchet derivatives. Recently, successful methods of crosstalk-free source encoding have been developed (Krebs et al., 2013; Huang & Schuster, 2012, 2017; Q. Zhang et al., 2018; Tromp & Bachmann, 2019; Bachmann & Tromp,

2020). In the approach of Q. Zhang et al. (2018) and Tromp and Bachmann (2019), encoded forward and adjoint wavefields are run until they reach a steady state, at which point they are 'decoded' – based on integration over a time interval that is the reciprocal of the encoded frequency spacing – to obtain their stationary parts. These parts are combined for all sources to obtain crosstalk-free Fréchet derivatives.

The main drawback of crosstalk-free source-encoded formulations arises from the difficulty of time windowing modeled data when inverting one or a few sparsely sampled frequencies at a time, and so selecting specific arrivals for the various stages of the inversion. To overcome this limitation, Z. Liu et al. (2023) and Cui et al. (2023) propose the use of complex-valued frequencies through the Laplace transform, which damp arrivals at a certain rate starting from a given traveltime. This approach focuses the inversion on first-arriving body waves and suppresses difficult-to-fit surface waves. As the iterations progress, the damping is gradually reduced, thereby blending in the later arrivals.

Model-order reduction: In model-order reduction (Rozza et al., 2008; Quarteroni et al., 2016) the system of equations for full waveform inversion is projected onto a lower dimensional space to reduce computational and memory requirements at the cost of introducing approximation errors. Hawkins et al. (2023) have recently demonstrated that model-order reduction shares similarities with classical normal-mode theory (Dahlen & Tromp, 1998). More generally, Hawkins et al. (2023) demonstrate how model-order reduction can be used for rapid calculations of seismograms in inverse problems, creating new opportunities for time-critical FWI applications.

Hamiltonian Monte Carlo sampling: The HMC method (Duane et al., 1987) is a Markov Chain Monte Carlo (MCMC) technique that uses derivatives of the probability density function to efficiently sample the posterior distribution (Neal, 2011; Betancourt, 2017). Thus, whereas MCMC requires just evaluations of the misfit, HMC also requires the misfit gradient, which may be accomplished based on the adjoint-state method used in traditional FWI. There are promising first applications of HMC techniques for tomography (Fichtner et al., 2019) and uncertainty quantification (Fichtner & Zunino, 2019).

In summary, I foresee many future opportunities for FWI across scales, for example, based on ultrasound for medical imaging and nondestructive testing or to probe the Earth's critical zone (Eppinger et al., 2023). In all such applications, crosstalk-free source

889 encoding and model-order reduction methods could be game-changers, especially when
890 combined with Bayesian inference accelerated by HMC techniques. Machine learning and
891 data analytics are likely to significantly impact FWI, especially in the contexts of data
892 assimilation and feature extraction.

FWI APPLICATION TO TELESEISMIC WAVES BENEATH DENSE ARRAYS (Qinya Liu)

The past two decades have witnessed growing applications of full-waveform inversion (FWI) techniques that generate high-resolution and high-fidelity images at both global and regional scales (see Tromp (2020) for a review). Most tectonic-scale FWI studies have relied on local earthquake data. But for seismic array deployments, FWI can also take advantage of other standard datasets used in seismic array analysis, particularly for regions with limited local seismicity. One such dataset is converted/scattered waves of teleseismic phases (referred to as *teleseismic waves* hereafter). Significant progress has been made in the past decade to apply FWI to teleseismic waves on dense arrays (TeleFWI). This approach is different from ray-based receiver function (RF) and inverse scattering approaches. To avoid the exorbitant numerical cost of full global simulation at teleseismic distances, TeleFWI uses hybrid methods to simulate the propagation of teleseismic waves (e.g., P) into a confined domain beneath an array (e.g., Monteiller et al., 2013; Tong et al., 2014) by interfacing 1D solvers with regional 3D solvers and can model high-frequency scattered waves down to $\sim 1-3$ s. The adjoint simulation and inversion iterations can be then carried out similarly as standard FWI practices.

TeleFWI has enabled some impressive fine-scale lithospheric imaging beneath dense array in recent years (e.g., Y. Wang et al., 2016; Beller et al., 2018; Kan et al., 2023). However it remains both encouraging and challenging in several aspects:

Datasets. Lithospheric imaging based on TeleFWI generally requires the station spacing to be $< 10-15$ km to avoid spatial aliasing, which largely restricts it to dense linear array deployments instead of regional 2D areal networks. On the other hand, as most temporary dense array deployments are just for 1-3 years, the requirement of coherent and slowly varying teleseismic waveforms across an array often severely limits the number of events (typically < 20) and the period band (typically ≥ 5 s) used in TeleFWI compared to tens to hundreds of events available for RF analysis and inverse scattering. Nevertheless, TeleFWI studies have successfully imaged lithospheric targets with only a handful of events, sometimes as few as five (Y. Wang et al., 2016). With recent theoretical development of finite-frequency kernels for receiver functions (de Jong et al., 2022), efforts have been made to use the deconvolved receiver functions themselves (Xu et al., 2023) which eliminates the need for source-time function estimation, improves the signal-to-noise ratio (SNR) of the inverted data and pushes the inverted period band down to

1-3 seconds. In addition to teleseismic SH waves (Kan et al., 2023), another dataset to explore is teleseismic SV scattered/converted waves used in S receiver functions. However, their limited epicentral distance range and lower SNR may result in even fewer usable events and therefore may only work when combined with other datasets.

Robustness Tests. Synthetic studies need to be conducted to further understand the robustness of TeleFWI or RF-based TeleFWI, such as the impact of initial models (Beller et al., 2018) and the presence of shallow/slow sedimentary basins. In particular, as TeleFWI still inverts for relatively smooth velocity variations, the connection to interfaces from RF needs to be better understood through well-designed synthetic experiments.

Joint inversions with ambient-noise data. For regions with both dense linear array and regional 2D arrays, TeleFWI has benefited from joint inversions with ambient noise data (K. Wang et al., 2021). While the practice of retrieving empirical Greens functions (EGFs) as another 'surface-wave' dataset for tomography has been challenged for non-homogeneous noise source distributions (e.g., Sager et al., 2020), EGFs have nevertheless been used widely in FWI-based imaging (e.g., Chen et al., 2014; X. Yang & Gao, 2020). The sensitivity of EGFs to the lithosphere is complementary to that of teleseismic waves and may significantly improve image resolutions at shallow depths. However, joint inversions will inevitably encounter issues of balancing datasets (e.g., body vs. surface waves) over multiple iterations and possible inconsistencies arising from fitting two different datasets. Better understanding of the sensitivity of these two datasets and the impact of non-homogeneous source distributions through a combination of synthetic tests and practical data examples may help provide some guidance for joint inversions.

Box tomography. The concept of TeleFWI can be extended to the *Box tomography* (e.g., Clouzet et al., 2018) approach if the imaging target is buried inside the Earth or in-between sources and receivers. Here the hybrid methods requie an additional step to extrapolate the wavefield from the local simulation domain back to the station at the surface for comparison with observed data (Pienkowska et al., 2021). Adaptation in the FWI framework with full-simulation-based Fréchet kernels may be feasible in the near future for array-based local fine-scale imaging of targets such as those in the transition zone or above the core-mantle boundary.

Despite these challenges, TeleFWI may soon become a standard FWI imaging technique applied to dense arrays deployed around the globe, such as those by the Earthscope Primary Instrument Center (EPIC). With elastic structures mapped to augment

959 images generated by standard array methods, TeleFWI allows more physical interpre-
960 tation of seismic images and hence help further address the underlying tectonic processes.

DENSE ARRAY, AMBIENT NOISE, AND RESOLVING DETAILED CRUSTAL STRUCTURE (Fan-Chi Lin)

Traditional high-resolution crustal imaging relies on dense recordings of high-frequency seismic signals excited by vibroseis or explosive sources. For such applications, close-spacing geophone sensors are deployed along lines to resolve detailed 2D reflection and refraction profiles. Conversely, passive seismic tomography studies tend to focus on resolving deeper and larger-scale Earth structures through broadband observations. Despite the less-than-optimal source and receiver distribution, researchers employ first-order approximations and regularizations to linearize and stabilize the inversion problem. Common approximations such as ray approximation and finite-frequency single scattering approximations work reasonably well when the model perturbation is small.

Despite the general interest in employing passive seismic tomography to resolve crustal structure—for applications ranging from energy and resource exploration to geohazard assessment and academic research—constructing high-resolution crustal models can be challenging due to the strong crustal heterogeneity. Notable examples include unconsolidated sediments within major sedimentary basins and partially molten magma reservoirs beneath volcanoes, which can cause seismic velocities to decrease by more than 30% compared to the surrounding bedrock and host rock. Such anomalies can introduce significant wavefield complexities, rendering first-order approximations inaccurate. Numerical tomographic methods (i.e., full waveform inversion) have been developed to improve the understanding of the wavefield and iteratively enhance the model constructed (Tromp et al., 2005; C. Tape et al., 2009). Nonetheless, the creation of a realistic reference starting model remains crucial for achieving rapid convergence and avoiding local minima in the model space.

In contrast to the numerical approach, an alternative approach to improve the understanding of a complex wavefield is to simply improve the receiver coverage. Recent developments in low-cost autonomous geophones have made this approach possible. These can-sized nodal geophones are self-contained, easy to deploy, and can record three-component passive seismic signals for over 30 days in a single deployment. While these geophone sensors are most sensitive to high-frequency signals, studies have demonstrated their ability to record short-period passive seismic signals relevant to crustal imaging (Y. Wang et al., 2019; Wilgus et al., 2023). As a result, deploying a large-N geophone array has become a practical solution to temporarily enhance data coverage in areas of interest.

Moreover, the deployment of a large-N array, combined with the source-receiver duality inherent to the noise cross-correlation method, not only improves receiver distribution but also enhances the source distribution. By cross-correlating noise time series recorded by a virtual source station and all other receiver stations across the array, a virtual wavefield can be constructed (Lin et al., 2013). While various studies have demonstrated the potential for extracting body wave energy from the noise correlation wavefield (e.g., Nakata et al., 2015; J. Castellanos et al., 2020), surface waves consistently represent the most energetic and robust signals. Empirical examination of the wavefield and solving the wave equation enable the direct measurement of various local surface wave properties, including group velocities, phase velocities, local amplification, and attenuation of Rayleigh and Love waves and Rayleigh wave ellipticity (Lin et al., 2013, 2014; Bowden et al., 2017). These measurements provide direct constraints on the underlying crustal velocity structure.

Despite the various degrees of success achieved in nodal experiments and ambient noise-based crustal imaging, numerous technical challenges remain to be addressed, offering promising research opportunities. The following is an incomplete list of topics that come to mind, though not intended to be exhaustive or unbiased. First, the characterization of the noise wavefield (i.e. diffusive, semi-diffusive, or non-diffusive) is essential for ambient noise applications. Unlike the ubiquitous presence of microseismic noise between 5 and 20 second period, noises at shorter periods are more sensitive to local noise excitation, which is often not well understood. Second, the presence of multi-mode surface wave interference can complicate the observed wavefield. Previous studies have demonstrated that higher-mode surface waves can be observed alongside the fundamental mode in areas in major sedimentary environments. Third, shallow crust may exhibit strong anisotropy due to structural foliation and crack alignment, where the often-assumed isotropic structure needs careful examination. Fourth, strong multi-scattering is expected near major lateral structural boundaries, and near-field interference between the forward and backscattering waves can be strong.

The pursuit of high-resolution crustal tomographic imaging is advancing through both numerical and empirical approaches. The deployment of large-N geophone arrays combined with ambient noise tomography offers significant promise for improving our understanding of Earth's shallow subsurface, but they also come with challenges that demand further research and innovation.

LEVERAGING INTERPRETIVE TOOLS TO BRIDGE TOMOGRAPHY AND GEOLOGY (Eva Golos)

Tomography has the potential to bridge geophysical observations and geologic processes. Other contributions in this work describe efforts towards the goal of quantitative interpretation of tomography that involve direct thermochemical inversion (e.g., Afonso et al., 2016; Fullea et al., 2021). An alternative approach combines seismically-determined wavespeed models with forward-modeling to infer thermal, chemical, and rheological properties (Goes & van der Lee, 2002; Cammarano et al., 2009). Implementation of the latter approach is facilitated by the recent development of interpretive toolkits that can be integrated into tomography workflows. In order to construct a well-posed problem that untangles the effects of multiple processes, these methods require models that constrain multiple geophysical parameters using multiple seismic observations.

One such toolkit is the Whole-Rock Interpretive Seismic Toolbox for Ultramafic Lithologies (WISTFUL) (Shinevar et al., 2022). WISTFUL selects the temperature and geochemical composition, defined by major-element oxide content, that best fit two out of three quantities (Vp, Vs, Vp/Vs). A correction is applied for the effects of anelasticity, but WISTFUL assumes no melting, so this tool is most appropriate for cratons and other settings where temperatures are well below the solidus. Shinevar et al. (2023) apply WISTFUL to determine continental-scale maps of temperature, Mg number, and density from the *MITPS_20* tomography model (Golos et al., 2020). The advantage to fitting temperature and composition from seismic wavespeed, rather than directly inverting seismic data for these properties, is that complicated mineral phase transitions are accounted for, particularly spinel-to-garnet, without needing empirical approximations. Also, by referencing mantle rock samples, the toolkit restricts interpretation to geologically feasible compositions. Drawbacks of WISTFUL include the absence of hydrated compositions, and lack of partial melt modeling.

A second interpretive tool is the Very Broadband Rheology calculator (VBRc) (Havlin et al., 2021). This calculator forward-models shear wavespeed and attenuation from temperature, melt fraction, and grain size. Four options are available for modeling anelastic effects on the temperature-velocity relationship. This tool is suitable for active tectonic settings where temperatures approach or exceed the solidus. Hopper et al. (2020) utilize VBRc to infer temperature and yield strength of the lithosphere below the East African Rift; Harmon et al. (2021) interpret partial melting below the Mid-Atlantic Ridge

from Vs and electrical resistivity structure. One obstacle is that Vs and attenuation are usually supplied by different models, which may differ in spatial resolution. Efforts should be made to use models with comparable spatial resolution, or to jointly invert for velocity and attenuation structure (e.g., H. Guo & Thurber, 2022). Furthermore, VBRc does not account for geochemical variations.

As interpretive toolkits gain traction within the community, several challenges must be addressed. Many tomography methods determine percentage perturbations in wavespeed, which must be converted to absolute values. Even models that do report absolute wavespeed are influenced by regularization operations such as damping and smoothing. A recent investigation reports that WISTFUL and VBRc temperature estimates can disagree by as much as $\sim$200°C using the same Vs (Golos et al., in prep.). In fact, variations on the order of $\sim$100°C exist within VBRc, depending on the choice of anelasticity model. Our understanding of the distribution of attenuation mechanisms, grain size, and melt geometry within the mantle is incomplete, with serious repercussions at the stage of interpretation. The modularization of interpretation within a software package allows mineral physics advances to be readily accommodated within an interpretive framework, without the need to re-run an entire tomographic inversion.

Uncertainty quantification remains a thorny issue. Interpreting geophysical model parameters, themselves obtained by inversion, inherently entails trade-offs. In WISTFUL, Vs is most sensitive to temperature (Goes & van der Lee, 2002), whereas Vp/Vs is sensitive to compositional variations as well (Shinevar et al., 2023). In VBRc, attenuation is not highly sensitive to melt fraction, though their relationship cannot be neglected (Havlin et al., 2021). Other geophysical and geochemical methods, including gravity, magnetotellurics, xenoliths, and magma thermobarometry, place further constraints on the parameters of interest.

Publicly-available toolkits such as WISTFUL and VBRc offer standardization across studies. If every research group has a proprietary interpretation tool, it is hard to replicate results and compare approaches. Do differences between interpretations arise from the seismic data used, from inversion approach, or from interpretive choices? This question can be addressed if the community coalesces around a set of common tools. Moreover, these toolkits enable interpretation of a wealth of previously-determined tomography models to answer geologic questions in myriad locales.

ANISOTROPY FROM CRYSTAL SCALE TO EARTH SCALE (Carl Tape)

Crystals that make up the solid Earth exhibit well-known crystallographic symmetries. Laboratory measurements, such as travel times of ultrasonic seismic waves, can be used to determine the elastic symmetry of crystals (Angel et al., 2009; Almqvist & Mainprice, 2017), and the elastic symmetry may differ from the crystallographic symmetry (Forte & Vianello, 1996). Elasticity is expressed by an elastic mapping $\mathbf{T}(\epsilon) = \sigma$ between 3×3 matrices of strain ϵ and stress σ. The elastic map $\mathbf{T}$ can be represented by a 6×6 symmetric matrix having 21 unique entries. Considering a single crystal, we ask the two questions: 1) What is the measured elastic anisotropy? 2) What is the true elastic anisotropy?

Consider a single crystal of olivine that has orthorhombic crystallographic symmetry and that has elastic symmetry to be determined. In a laboratory setting, it would be best to measure all 21 elastic parameters, including uncertainties. The measured elastic parameters would almost certainly imply only trivial elastic symmetry, meaning that the only rotational symmetry of $\mathbf{T}$ is the identity matrix. But, within the measurement uncertainties, orthorhombic elastic symmetry might well be a possibility. However, most compilations of single-crystal elastic constants show values (and without uncertainties) that are confined to specific symmetry classes (Almqvist & Mainprice, 2017). An exception would be Brown et al. (2016), who lists all 21 parameters, with uncertainties, for a set of feldspar crystals.

Anisotropy in the Earth extends to much larger scales, such as a sample of shale rock (Christensen & Mooney, 1995), a crustal metamorphic terrane (Okaya et al., 2004), or a region of uppermost mantle (Maupin & Park, 2007). Toward the future, we can hope for ideal data coverage for making measurements of anisotropy: complete coverage around a laboratory sample of rock, dense (10 m spacing) surface coverage of seismic sensors along with many fully instrumented boreholes for a kilometer-scale portion of the uppermost crust, dense (10 km spacing) seismic station coverage of the entire planet (land and sea). Recording traveltimes of waves through these materials enables characterization of the anisotropic structure of the medium. To achieve this, measurements must be taken for all possible paths through each portion of the material, and all measurements must have associated uncertainties. For the estimation side, it would be best to not assume anything regarding the elastic symmetry of the material: that is, assume trivial symmetry.

For real-Earth seismic imaging, we seldom have ideal coverage, and we are also faced with a highly heterogeneous material. Therefore, we tend to assume that the elastic material has some non-trivial symmetry, such as either isotropic or transverse isotropic with vertical, horizontal, or arbitrary symmetry axis. This reduces the number of unknown parameters at each point in the Earth from 21 to 2, 5, 6, or 7.

Figure 6 provides a framework for visualizing the reductions that are commonly made in seismology and that are implicitly made in compilations of single-crystal elasticity (Almqvist & Mainprice, 2017). While a true material might have, or be measured to have, trivial symmetry (the ball at the bottom), we might want to assume that the material is isotropic or transversely isotropic (balls at top left). With improvements in data coverage, measurements, computational resources, and algorithms for seismic imaging, we might instead assume that every single crystal in a laboratory and every 'cell' in a tomographic model has 21 parameters. With proper handling of measurement uncertainties, these 21 parameters can be estimated from the measurements, and then the question can be asked after the fact: What is the likely elastic symmetry of the material? This approach is currently more tractable at a single-crystal scale, but it seems possible for the future of seismic imaging.

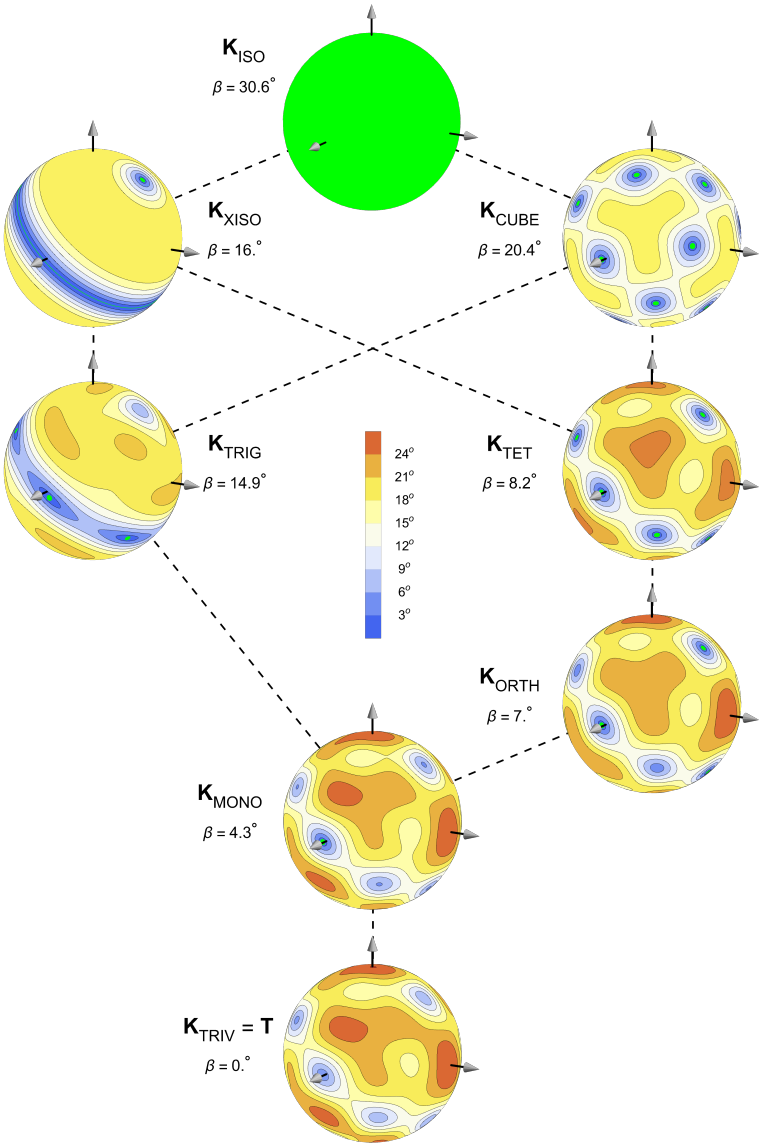


Figure 6. An elastic map $\mathbf{T}$ and a closest map $\mathbf{K}_\Sigma$ to it having symmetry Σ (trivial, monoclinic, orthorhombic, tetragonal, trigonal, cubic, transverse isotropic, isotropic). Each map $\mathbf{K} = \mathbf{K}_\Sigma$ is depicted as the contour map of its "monoclinic angle function" $\alpha^{\mathbf{K}}_{\mathrm{MONO}}$ (W. Tape & Tape, 2022). For a point $\mathbf{v}$ on the sphere, $\alpha^{\mathbf{K}}_{\mathrm{MONO}}(\mathbf{v})$ is the angle between $\mathbf{K}$ and the closest elastic map to $\mathbf{K}$ having a 2-fold symmetry axis at $\mathbf{v}$. The green points are where $\alpha^{\mathbf{K}}_{\mathrm{MONO}} = 0$ (inconsistent with the color scale) and are therefore the 2-fold axes of $\mathbf{K}$. They determine the symmetry group of $\mathbf{K}$, which is also seen in the contour plot itself. In this example, $\mathbf{T}$ has trivial symmetry and is from Igel et al. (1995); it is $\beta = 4.3°$ from being monoclinic and is $\beta = 30.6°$ from being isotropic.

IMPLICATIONS OF VISCOELASTIC RAY THEORY FOR ANELASTIC SEISMIC TOMOGRAPHY (Roger D. Borcherdt)

The anelastic conversion of kinetic and potential energy into heat is an important aspect of seismic wave propagation in a layered anelastic Earth. It can be one of the major contributors to larger amounts of apparent attenuation of lower frequency seismic waves. Inference of the properties and distribution of anelastic Earth materials is fundamental to understanding the internal composition of the Earth (Anderson & Archambeau, 1966; Romanowicz & Mitchell, 2015).

Standard anelastic models provide valuable estimates of the Earth's anelastic structure as inferred from average estimates of attenuation along ray paths predicted for P and S waves by elastic ray theory. Recent insights provided by viscoelastic ray theory predict that P and S waves refract across anelastic boundaries with contrasts in anelastic material absorption as inhomogeneous waves with corresponding changes in the wave's speed, attenuation, and trajectory. To account for these effects on seismic waves, especially in areas with high intrinsic material absorption, full implementation of viscoelastic ray theory is needed. A current challenge is to incorporate recent developments in viscoelastic wave-propagation and ray theory into tomographic inversion procedures.

Viscoelasticity provides an infinite number of phenomenological constitutive models that can be used to describe linear anelastic material behavior (Bland, 1960; Gurtin & Sternberg, 1962; Volterra, 2005). Its general formulation affords exact anelastic ray-tracing computation algorithms and general anelastic solutions to many of the monochromatic body- and surface-wave problems of seismology, as well as solutions of simple inverse problems to simultaneously infer intrinsic material velocity and intrinsic anelastic material absorption from simultaneous measurements of travel time and amplitude (Borcherdt, 2020).

In the presence of significant contrasts and amounts of anelasticity, a variety of wave characteristics are modified from those for elastic waves. For example, in an anelastic multilayered medium properties of refracted anelastic P and S waves, such as phase and energy speed, trajectory, particle motion, and amplitude are predicted to vary with angle of incidence whereas they are invariant for an elastic medium. Refracted anelastic waves are predicted to travel at slower wave speeds and refract at steeper angles of incidence than for elastic waves, which results in anelastic ray paths with travel times and

distances distinct from those for elastic waves. In addition, the theoretical solutions predict the existence of two types of anelastic inhomogeneous S waves (SI , SII) with distinct elliptical and linear particle motions and distinct reciprocal quality factors.

Numerical results indicate that an important manifestation of these effects is the refraction of energy across anelastic boundaries as a head-wave and as Wide Angle Refracted (WAR) waves (Borcherdt, 2020). These anelastic waves, which are not predicted by elastic ray theory, are confirmed by laboratory measurements and numerical models. Interpretations of the travel times and amplitudes of reflected WAR waves, where they are observable, are expected to provide new insights at major anelastic discontinuities for comparison with those of standard reference models such as *PREM* (Dziewoński & Anderson, 1981) and *ak135* (Kennett et al., 1995)

Near-surface seismic recordings of displacement and volumetric strain provide additional empirical evidence in confirmation of theoretically-predicted characteristics of anelastic seismic waves (Borcherdt et al., 1989). In general, they confirm that the largest differences between anelastic and elastic waves in layered media occur for near-critical and wide-angles of incidence. For precritical angles of incidence they confirm that notable differences in amplitude exist, but travel time differences are small and well approximated by those inferred for elastic seismic models.

In the context of the conference theme *Seismic Tomography, What Comes Next*?, the general viscoelastic solutions of the fundamental wave-propagation and ray-theory problems for seismology provide a theoretical framework for anelastic seismic tomography. Viscoelastic computation algorithms readily permit the development of general exact ray tracing codes for body waves that account for the effect of anelastic boundaries on the travel times, amplitudes, and trajectories of seismic waves for all angles of incidence, including those for head waves and WAR waves. Their full implementation for horizontal and spherical tomography remains to be completed, but when applied to large exploration and teleseismic data sets, they are expected to reveal new insights regarding the thermo-chemical structure of the Earth's interior over a range of spatial scales.

MULTIPHYSICS ADJOINT TOMOGRAPHY OF PORE SCALE PHENOMENA (Christina Morency)

For the past decades, adjoint tomography has had tremendous successes for regional (e.g., C. Tape et al., 2009; Zhu et al., 2015; Tao et al., 2018; Rodgers et al., 2022) and global (e.g., Bozdağ et al., 2016; Lei et al., 2020) applications, due in large part to the development of high-performance computing and effective numerical methods (Komatitsch & Vilotte, 1998; Komatitsch & Tromp, 1999). For reservoir scale applications, such as oil & gas recovery, geothermal, and carbon storage monitoring, subsurface seismic imaging techniques have (1) slowly evolved from purely acoustic to elastic formulations and (2) from focusing on interfaces detections to properties characterization.

In each of these reservoir scale applications, fluid circulation in a porous and sometimes fractured medium is involved, and the main goal of subsurface imaging is to be able to track, monitor, and characterize pore fluid properties and fracture networks. Common approaches for subsurface imaging rely predominantly on seismic techniques, using acoustic or elastic rheologies, which alone do not directly capture pore fluid properties and related mechanisms. Using Gassmann's formulae (Gassmann, 1951), which relate effective bulk and shear moduli of dry rock to effective moduli of the same rock saturated with fluid, one can only approximate some fluid properties and, in essence, still remain in a seismic elastic paradigm. Even a full seismic poroelastic adjoint approach, based on Biot's formulation (Biot, 1956a, 1956b), does not allow efficient access to fluid properties other than fluid bulk modulus and fluid density (Morency et al., 2011). This is in part because seismometers measure solid displacements and offer few direct constraints on the fluid phase. Another geophysical technique, favored to characterize fluid properties such as resistivity and permeability, is based on electromagnetic (EM) methods. EM measurements add direct constraints on the fluid phase, but EM signals alone do not offer information on the rock properties. In the last decades, there have been efforts to combine both seismic and EM datasets for exploration geophysics. The most popular approach is based on joint inversion of seismic and EM datasets, as decoupled phenomena, to recover seismic velocity and electrical resistivity (e.g., Hoversten et al., 2006; Hu et al., 2009; Colombo & Rovetta, 2018).

However, back in the 1930's, Ivanov's observations showed that ground motion triggered by a seismic source propagating in a porous medium generates an electric field due to electrokinetic forces at the pore scale, underlying the natural coupling of seismic and

EM phenomena (Ivanov, 1939). We have to wait until the 1990s and later, for theoretical and experimental development of what are known as the seismoelectric effects, with first field data collected and analyzed by Thompson and Gist (1993), experimental studies by e.g., Mikhailov et al. (2000); Bordes et al. (2015); Martins Gomes (2022), and the rise of numerical modeling supported by Pride's formulation (Pride, 1994) based on the coupled Biot poroelastic seismic and Maxwell electromagnetic wave equations (e.g., Haines & Pride, 2006; Revil & Jardani, 2010; Meyer, 2021; Morency & Matzel, 2021).

A natural next step is tackling the inverse problem. However, existing literature on the inversion of seismoelectric datasets is not extensive. The most notable and, to my knowledge, first work on seismoelectric signal inversion is based on a probabilistic approach, where Jardani et al. (2010) developed and conducted a stochastic joint inversion of synthetic seismic and seismoelectric datasets, using an Adaptive Metropolis algorithm. Considering two flat layers plus a rectangular reservoir embedded in the second layer 2D geometry, they were able to recover the permeability within one order of magnitude, and the electrical conductivity and poroelastic mechanical properties were well resolved, but the porosity wasn't well constrained. Several studies have focused on sensitivity analysis, impact of signal-to-noise-ratio, and they show that the inversion of seismoelectric data alone performed better than that of seismic data alone, and that the joint inversion of both seismic and seismoelectric datasets offers the best resolution of electric and poroelastic model parameters (Mahardika et al., 2012; Macchioli-Grande et al., 2020).

Seismoelectric inversion has the potential to combine the resolution and depth of penetration of seismic techniques with the sensitivity of EM techniques to pore fluid properties. I believe that the adjoint method can be as big a game changer for seismoelectric signals inversion as it has been for seismic tomography. That is why the work by Morency and Matzel (2021), based on a spectral-element method to resolve seismoelectric effects, is forging the path toward joint adjoint inversion of seismic and electric properties using seismoelectric datasets, leveraging the SPECFEM package and previous work on adjoint seismic tomography. There is still a lot of room for research on seismoelectric data acquisition, processing and inversion to demonstrate practical use of this technique (Morency et al., 2022), which should keep on opening future areas of work on these exciting pore-scale phenomena.

Conclusions

Seismic Tomography 2023 offers a snapshot of modern seismic tomography with a focus on outstanding challenges and particularly promising research directions. Written by an experienced group of authors, it is intended to guide not only other Earth science professionals but also young students who wish to develop their own research in this exciting field.

While a superficial look at the individual contributions may give the impression that their topics are scattered and disconnected, a more careful read reveals a small number of coherent threads. The diversity is only apparent, and often topics are just seen from different angles, influenced by personal preferences and variable experience.

Simply counting how often a topic is mentioned, possibly in different disguises, the most prominent challenges seem to be two closely related classics: (1) data quality and quantity, especially in the oceans and the southern-hemisphere continents, and (2) multi-parameter inversion in a broader sense, including not only anisotropy and attenuation but also poro-elastic parameters. Clearly, (1) is the most obvious, though certainly not the easiest, approach to making progress on (2).

Several other, frequently mentioned topics can be understood in the context of these two: (3) Multi-parameter inversion increases the importance of inter-parameter trade-offs, thereby amplifying the need for careful uncertainty quantification. Despite major efforts, uncertainty quantification is still considered by many an open problem, not only due to limited computational resources, but also partly because rather technical uncertainty proxies may not be particularly useful in geologic interpretations. (4) Reformulation of tomographic problems so that hypothesis testing of geological and geodynamic issues replaces comprehensive uncertainty quantification that is often infeasible in practice. (5) Further advancing full-waveform inversion to optimally exploit information in seismic recordings is considered one of the most promising approaches towards multi-parameter inversion and the reduction of uncertainties. The most critical advance is the increase of frequency bandwidth, and related developments in numerical wave propagation, high-performance computing and non-linear optimization. (6) Last but not least, future progress in seismic tomography hinges on more careful presentations of our models in order to facilitate quantitative comparisons. While uncertainty quantification would be an important step towards a better comparability of models, there may be much more

low-hanging fruit, including the presentation of absolute seismic wave speeds, the omission of the 210 km discontinuity from initial models, or the low-pass filtering of different models to produce images of comparable spatial resolution.

This paper should be interpreted as a document of its time and a reference point for future developments. It remains to be seen which of the major problems will be considered solved, to some extent, in *Seismic Tomography 2033*.

Data and resources

No data have been used for this manuscript.

Competing interests

None of the authors has competing interests.

Acknowledgments

The authors gratefully acknowledge invaluable support provided by the Seismological Society of America, and in particular by Nan Broadbent and Rikki Anderson, during the organisation of the 2022 Seismic Tomography conference in Toronto. Countless discussions and intresting presentations made the meeting a real success. Contribution of AR and CM prepared by LLNL under Contract DE-AC52-07NA27344. EB acknowledges the support by the National Science Foundation (NSF) under Award No. EAR1945565 and Texas Advanced Computing Center (TACC) at the University of Texas at Austin for providing computational resources on Frontera system (Stanzione et al., 2020) through allocation EAR21003 (www.tacc.utexas.edu). SL acknowledges support from the Natural Environment Research Council (NERC), UK, under grant XE/X000060/1. VCT acknowledges support from NSF grant EAR-2011079.

References

Adourian, S., Lyu, C., Masson, Y., Munch, F., & Romanowicz, B. (2021). Combining different 3D global and regional seismic wave propagation solvers towards box tomography in the deep Earth. *Geophys. J. Int.*, *232*, 1340–1356.

Afanasiev, M., Boehm, C., van Driel, M., Krischer, L., Rietmann, M., May, D. A., ... Fichtner, A. (2019). Modular and flexible spectral-element waveform mod-

elling in two and three dimensions. *Geophys. J. Int.*, *216*(3), 1675–1692. doi: 10.1093/gji/ggy469

Afonso, J. C., Rawlinson, N., Yang, Y., Schutt, D. L., Jones, A. G., Fullea, J., & Griffin, W. L. (2016). 3-D multiobservable probabilistic inversion for the compositional and thermal structure of the lithosphere and upper mantle: III. Thermochemical tomography in the Western-Central U.S. *J. Geophys. Res.*, *121*(10), 7337–7370. doi: 10.1002/2016JB013049

Aki, K., Christoffersson, A., & Husebye, E. S. (1977). Determination of three-dimensional seismic structure of the lithosphere. *J. Geophys. Res.*, *81*, 277–296. doi: 10.1029/JB082i002p00277

Aki, K., & Lee, W. H. K. (1976). Determination of three-dimensional velocity anomalies under a seismic array using first P arrival times from local earthquakes - 1. A homogeneous initial model. *J. Geophys. Res.*, *81*, 4381–4399. doi: 10.1029/JB081i023p04381

Almqvist, B. S. G., & Mainprice, D. (2017). Seismic properties and anisotropy of the continental crust: Predictions based on mineral texture and rock microstructure. *Rev. Geophysics*, *55*, 367–433. doi: 10.1002/2016RG000552

Anderson, D. L. (1967). The anelasticity of the mantle. *Geophys. J. R. Astr. Soc.*, *14*, 135–164.

Anderson, D. L., & Archambeau, C. B. (1966). The anelasticity of the Earth. *J. Geophys. Res.*, *69*, 2071–2084.

Angel, R. J., Jackson, J. M., Reichmann, H. J., & Speziale, S. (2009). Elasticity measurements on minerals: a review. *European J. Mineraology*, *21*, 525–550. doi: 10.1127/0935-1221/2009/0021-1925

Austermann, J., Mitrovica, J. X., Latychev, K., & Milne, G. A. (2013). Barbados-based estimate of ice volume at last glacial maximum affected by subducted plate. *Nature Geoscience*, *6*, 553–557.

Bachmann, E., & Tromp, J. (2020). Source encoding for viscoacoustic ultrasound computed tomography. *J. Acoust. Soc. Am.*, *147*(5), 3221–3235.

Backus, G. E., & Gilbert, F. (1970). Uniqueness in the inversion of inaccurate gross Earth data. *Phil. Trans. R. Soc. A*, *266*, 123–192.

Bamberger, A., Chavent, G., & Lailly, P. (1977). Une application de la théorie du contrôle à un problème inverse sismique. *Ann. Geophys.*, *33*, 183–200.

1358 Bartzsch, S., Lebedev, S., & Meier, T. (2011). Resolving the lithosphere–
1359 asthenosphere boundary with seismic Rayleigh waves. *Geophys. J. Int.*, *186*(3),
1360 1152–1164.

1361 Beller, S., Monteiller, V., Operto, S., Nolet, G., Paul, A., & Zhao, L. (2018). Litho-
1362 spheric architecture of the South-Western Alps revealed by multiparameter
1363 teleseismic full-waveform inversion. *Geophys. J. Int.*, *212*, 1369–1388.

1364 Ben-Hadj-Ali, H., Operto, S., & Virieux, J. (2009). An efficient frequency-domain
1365 full waveform inversion method using simultaneous encoded sources. *Geo-*
1366 *physics*, *76*, R109–R124.

1367 Bernauer, M., Fichtner, A., & Igel, H. (2014). Optimal observables for multi-
1368 parameter seismic tomography. *Geophys. J. Int.*, *198*, 1241–1254.

1369 Betancourt, M. (2017). A conceptual introduction to Hamiltonian Monte Carlo.
1370 *arXiv:1701.02434*.

1371 Bianchi, M. B., Assumpção, M., Rocha, M. P., Carvalho, J. M., Azevedo, P. A.,
1372 Fontes, S. L., ... Costa, I. S. L. (2018). The Brazilian Seismographic Net-
1373 work (RSBR): Improving Seismic Monitoring in Brazil. *Seis. Res. Lett.*, *89*,
1374 452—457. doi: 10.1785/0220170227

1375 Bijwaard, H., Spakman, W., & Engdahl, E. R. (1998). Closing the gap between re-
1376 gional and global traveltime tomography. *J. Geophys. Res.*, *103*, 30055-30078.

1377 Biot, M. A. (1956a). Theory of propagation of elastic waves in a fluid-saturated
1378 porous solid. II Higher frequency range. *J. Acoust. Soc. Am*, *28*, 179–191.

1379 Biot, M. A. (1956b). Theory of propagation of elastic waves in a fluid-saturated
1380 porous solid. I Low-frequency range. *J. Acoust. Soc. Am*, *28*, 168–178.

1381 Bland, D. R. (1960). *The Theory of Linear Viscoelasticity.* Pergamon Press, New
1382 York.

1383 Bodin, T., & Sambridge, M. (2009). Seismic tomography with the reversible jump
1384 algorithm. *Geophys. J. Int.*, *178*, 1411–1436.

1385 Bodin, T., Sambridge, M., Rawlinson, N., & Arroucau, P. (2012). Transdimensional
1386 tomography with unknown data noise. *Geophys. J. Int.*, *189*, 1536–1556.

1387 Bonadio, R., Lebedev, S., Meier, T., Arroucau, P., Schaeffer, A. J., Licciardi, A., ...
1388 Ireland Array Working Group (2021). Optimal resolution tomography with
1389 error tracking and the structure of the crust and upper mantle beneath Ireland
1390 and Britain. *Geophys. J. Int.*, *226*(3), 2158–2188.

Borcherdt, R. D. (2020). *Viscoelastic Waves and Rays in Layered Media.* Cambridge University Press, Cambridge, U. K.

Borcherdt, R. D. (2024). Preliminary implications of viscoelastic ray theory for anelastic seismic tomography models. *Bull. Seis. Soc. Am.*, in press.

Borcherdt, R. D., Johnston, M. J. S., & Glassmoyer, G. (1989). On the use of volumetric strain meters to infer additional characteristics of short-period seismic radiation. *Bull. Seism. Soc. Am.*, *79*, 1006–1023.

Bordes, C., Sénéchal, P., Barrière, J., Brito, D., Normandin, E., & Jougnot, D. (2015). Impact of water saturation on seismoelectric transfer functions: a laboratory study of coseismic phenomenon. *Geophys. J. Int.*, *200*(3), 1317–1335.

Bowden, D. C., Tsai, V. C., & Lin, F.-C. (2017). Amplification and attenuation across USArray using ambient noise wavefrom tracking. *J. Geophys. Res.*, *122*, doi:10.1002/2017JB014804.

Bozdağ, E., Peter, D., Lefebvre, M., Komatitsch, D., Tromp, J., Hill, J., ... Pugmire, D. (2016). Global adjoint tomography: first-generation model. *Geophys. J. Int.*, *207*(3), 1739–1766.

Brown, J. M., Angel, R. J., & Ross, N. L. (2016). Elasticity of plagioclase feldspars. *J. Geophys. Res. Solid Earth*, *121*, 663–675. doi: 10.1002/2015JB012736

Bunge, H.-P., & Richards, M. A. (1996). The origin of large scale structure in mantle convection: effects of plate motions and viscosity stratification. *Geophys. Res. Lett.*, *23*, 2987–2990.

Cammarano, F., Romanowicz, B., Stixrude, L., Lithgow-Bertelloni, C., & Xu, W. (2009). Inferring the thermochemical structure of the upper mantle from seismic data. *Geophys. J. Int.*, *179*(2), 1169–1185. doi: 10.1111/j.1365-246X.2009.04338.x

Cammarano, F., Tackley, P., & Boschi, L. (2011). Seismic, petrological and geodynamical constraints on thermal and compositional structure of the upper mantle: global thermochemical models. *Geophys. J. Int.*, *187*, 1301–1318.

Capdeville, Y., Larmat, C., Vilotte, J. P., & Montagner, J. P. (2002). A new coupled spectral element and modal solution method for global seismology: A first application to the scattering induced by a plume-like anomaly. *Geophys. Res. Lett.*, *29*, 32-1–32-4. doi: 10.1029/2001GL013747

Carmona, A. E., Peter, D., Parisi, L., & Mai, P. M. (2024). Anelastic tomography of

the Arabian Plate. *Bull. Seis. Soc. Am.*, in press.

Castellanos, C., Métivier, L., Operto, S., Brossier, R., & Virieux, J. (2015). Fast full waveform inversion with source encoding and second-order optimization methods. *Geophys. J. Int.*, *200*, 718–742.

Castellanos, J., Clayton, R., & Juarez, A. (2020). Using a time-based subarray method to extract and invert noise-derived body waves at long beach, california. *J. Geophys. Res.*, *125*(5), e2019JB018855.

Castelvecchi, D. (2017). Long-awaited mathematics proof could help scan Earth's innards. *Nature*, *542*, 281–282.

Chaves, C. A. M., Ritsema, J., & Koelemeijer, P. (2020). Comparing ray-theoretical and finite-frequency teleseismic traveltimes: implications for constraining the ratio of s-wave to p-wave velocity variations in the lower mantle. *Geophys. J. Int.*, *224*, 1540—1552. doi: 10.1093/gji/ggaa534

Chen, M., Huang, H., Yao, H. J., van der Hilst, R. D., & Niu, F. L. (2014). Low wave speed zones in the crust beneath SE Tibet revealed by ambient noise adjoint tomography. *Geophys. Res. Lett.*, *41*, 334–340.

Choi, Y., & Alkhalifah, T. (2011). Source-independent time-domain wave-form inversion using convolved wavefields. *Geophysics*, *76*, R125–R134.

Chow, B., Kaneko, Y., Tape, C., Modrak, R., & Townend, J. (2020). An automated workflow for adjoint tomography—waveform misfits and synthetic inversions for the North Island, New Zealand. *Geophys. J. Int.*, *223*(3), 1461–1480. doi: 10.1093/gji/ggaa381

Christensen, N. I., & Mooney, W. D. (1995). Seismic velocity structure and composition of the continental crust: A global view. *J. Geophys. Res.*, *100*(B7), 9761–9788.

Civiero, C., Lebedev, S., Xu, Y., Bonadio, R., & Lavoué, F. (2024). Toward tectonic-type and global 1D seismic models of the upper mantle constrained by broadband surface waves. *Bull. Seis. Soc. Am.*, in press.

Clouzet, P., Masson, Y., & Romanowicz, B. (2018). Box Tomography: First application to the imaging of upper-mantle shear velocity and radial anisotropy structure beneath the North American continent. *Geophys. J. Int.*, *213*, 1849–1875.

Colombo, D., & Rovetta, D. (2018). Coupling strategies in multiparameter geophysi-

cal joint inversion. *Geophys. J. Int.*, *215*(2), 1171–1184.

Connolly, J. A. (2005). Computation of phase equilibria by linear programming: a tool for geodynamic modeling and its application to subduction zone decarbonation. *Earth Planet. Sci. Lett.*, *236*(1-2), 524–541.

Cottaar, S., & Lekic, V. (2016). Morphology of seismically slow lower-mantle structures. *Geophys. J. Int.*, *207*, 1122–1136.

Cui, C., Bachmann, E., Peter, D., Liu, Z., & Tromp, J. (2023). Source-encoded waveform inversion of the Northern Hemisphere. *Geophys. J. Int.* (Submitted.)

Cupillard, P., Delavaud, E., Burgos, G., Festa, G., Vilotte, J.-P., Capdeville, Y., & Montagner, J.-P. (2012). RegSEM: a versatile code based on the spectral element method to compute seismic wave propagation at the regional scale. *Geophys. J. Int.*, *188*, 1203–1220.

Dahlen, F. A., Hung, S.-H., & Nolet, G. (2000). Fréchet kernels for finite-frequency traveltimes – I. Theory. *Geophys. J. Int.*, *141*, 157–174.

Dahlen, F. A., & Tromp, J. (1998). *Theoretical Global Seismology.* New Jersey: Princeton University Press.

Dalton, C. A., Ekström, G., & Dziewonski, A. M. (2008). The global attenuation structure of the upper mantle. *J. Geophys. Res.*, *113*. doi: 10.1029/2007JB005429

Debayle, E., & Ricard, Y. (2012). A global shear velocity model of the upper mantle from fundamental and higher Rayleigh mode measurements. *J. Geophys. Res.*. doi: 10.1029/2012JB009288

de Jong, J. H. E., Paulssen, H., van Leeuwen, T., & Trampert, J. (2022). Sensitivity kernels for receiver function misfits in a full waveform inversion workflow. *Geophys. J. Int.*, *230*, 1065–1079. doi: 10.1093/gji/ggac098

Del Piccolo, G., VanderBeek, B. P., Faccenda, M., Morelli, A., & Byrnes, J. (2024). Imaging upper mantle anisotropy with trans-dimensional Bayesian Monte Carlo sampling. *Bull. Seis. Soc. Am.*, in press.

Donini, A., Palomares-Ruiz, S., & Salvado, J. (2019). Neutrino tomography of Earth. *Nature Phys.*, *15*, 37–40.

Duane, S., Kennedy, A. D., Pendleton, B. J., & Roweth, D. (1987). Hybrid Monte Carlo. *Phys. Lett. B*, *195*, 216–222.

Durek, J. J., & Ekström, G. (1996). A radial model of anelasticity consistent with long-period surface wave attenuation. *Bull. Seism. Soc. Am.*, *86*, 144–158.

Dziewonski, A. M. (1984). Mapping the lower mantle: determination of lateral heterogeneity in p velocity up to degree and order 6. *J. Geophys. Res.*, *89*, 5929–5952.

Dziewoński, A. M., & Anderson, D. L. (1981). Preliminary Reference Earth Model. *Phys. Earth Planet. Inter.*, *25*, 297–356. doi: 10.1016/0031-9201(81)90046-7

Dziewonski, A. M., & Anderson, D. L. (1984). Seismic Tomography of the Earth's Interior: The first three-dimenstional models of the earth's structure promise to answer some basic questions of geodynamics and signify a revolution in earth science. *American Scientist*, *72*, 483-494.

Dziewoński, A. M., Hager, B. H., & O'Connell, R. J. (1977). Large-scale heterogeneities in the lower mantle. *J. Geophys. Res.*, *82*, 239–255.

Eberhart-Phillips, D., & Fry, B. (2017). A new scheme for joint surface wave and earthquake travel-time inversion and resulting 3-D velocity model for the western North Island, New Zealand. *Phys. Earth Planet. Inter.*, *269*, 98–111. doi: 10.1016/j.pepi.2017.05.014

Ekström, G., & Dziewonski, A. M. (1998). The unique anisotropy of the Pacific upper mantle. *Nature*, *394*, 168–172.

Eppinger, B. J., Holbrook, W. S., Liu, Z., Flinchum, B. A., & Tromp, J. (2023). Near-surface full-waveform inversion reveals bedrock controls on critical zone architecture. *J. Geophys. Res.*. (Submitted.)

Fang, H., van der Hilst, R. D., de Hoop, M. V., Kothari, K., Gupta, S., & Dokmanić, I. (2019). Parsimonious seismic tomography with Poisson Voronoi projections: Methodology and validation. *Seism. Res. Lett.*, *91*(1), 343–355. doi: 10.1785/0220190141

Fang, H., Zhang, H., Yao, H., Allam, A., Zigone, D., Ben-Zion, Y., ... van der Hilst, R. D. (2016). A new algorithm for three-dimensional joint inversion of body wave and surface wave data and its application to the Southern California plate boundary region. *J. Geophys. Res. Solid Earth*, *121*, 3557–3569. doi: 10.1002/2015JB012702

Fichtner, A. (2010). *Full Seismic Waveform Modelling and Inversion.* Springer, Heidelberg.

Fichtner, A., Bunge, H.-P., & Igel, H. (2006). The adjoint method in seismology: I. theory. *Phys. Earth Planet. Inter.*, *157*(1), 86–104. doi: 10.1016/j.pepi.2006.03.016

Fichtner, A., Kennett, B. L. N., Igel, H., & Bunge, H.-P. (2009). Full seismic waveform tomography for upper-mantle structure in the Australasian region using adjoint methods. *Geophys. J. Int.*, *179*, 1703–1725.

Fichtner, A., & Trampert, J. (2011). Hessian kernels of seismic data functionals based upon adjoint techniques. *Geophys. J. Int.*, *185*, 775–798.

Fichtner, A., van Herwaarden, D., Afanasiev, M., Simute, S., Krischer, L., Cubuk-Sabuncu, Y., ... Igel, H. (2018). The Collaborative Seismic Earth Model: Generation I. *Geophys. Res. Lett.*, *45*, 4007–4016.

Fichtner, A., & Zunino, A. (2019). Hamiltonian nullspace shuttles. *Geophys. Res. Lett.*, *46*, 644–651.

Fichtner, A., Zunino, A., & Gebraad, L. (2019). Hamiltonian Monte Carlo solution of tomographic inverse problems. *Geophys. J. Int.*, *216*, 1,344–1,363. doi: 10.1093/gji/ggy496

Forte, S., & Vianello, M. (1996). Symmetry classes for elasticity tensors. *J. Elasticity*, *43*, 81–108.

French, S. W., & Romanowicz, B. A. (2014). Whole-mantle radially anisotropic shear velocity structure from spectral-element waveform tomography. *Geophys. J. Int.*, *199*, 1303–1327.

French, S. W., & Romanowicz, B. A. (2015). Broad plumes rooted at the base of the Earth's mantle beneath major hotspots. *Nature*, *525*, 1303–1327.

Fullea, J., Lebedev, S., Agius, M., Jones, A., & Afonso, J. C. (2012). Lithospheric structure in the Baikal–central Mongolia region from integrated geophysical-petrological inversion of surface-wave data and topographic elevation. *Geochemistry, Geophysics, Geosystems*, *13*(8).

Fullea, J., Lebedev, S., Martinec, Z., & Celli, N. (2021). WINTERC-G: mapping the upper mantle thermochemical heterogeneity from coupled geophysical–petrological inversion of seismic waveforms, heat flow, surface elevation and gravity satellite data. *Geophys. J. Int.*, *226*(1), 146–191.

Gassmann, F. (1951). Uber die Elastizitat poroser Medien. *Vier, der Natur, Gesellschaft in Zurich*, *96*, 1–23.

Goes, S., & van der Lee, S. (2002). Thermal structure of the North American uppermost mantle inferred from seismic tomography. *J. Geophys. Res.*, *107*(B3), ETG 2-1–ETG 2-13. doi: 10.1029/2000JB000049

Golos, E. M., Fang, H., & van der Hilst, R. D. (2020). Variations in Seismic Wave Speed and VP/VS Ratio in the North American Lithosphere. *Journal of Geophysical Research: Solid Earth*, *125*(12), e2020JB020574. doi: 10.1029/2020JB020574

Gorbatov, A., & Kennett, B. L. N. (2003). Joint bulk-sound and shear tomography for Western Pacific subduction zones. *Earth Planet. Sci. Lett.*, *210*, 527–543.

Guo, H., & Thurber, C. (2022). Temporal Changes in Seismic Velocity and Attenuation at The Geysers Geothermal Field, California, From Double-Difference Tomography. *Journal of Geophysical Research: Solid Earth*, *127*(5), e2021JB022938. doi: 10.1029/2021JB022938

Guo, Z., & Zhou, Y. (2019). Finite-frequency imaging of the global 410- and 660-km discontinuities using SS precursors. *Geophys. J. Int.*, *220*, 1978–1994. doi: 10.1093/gji/ggz546

Gurtin, M. E., & Sternberg, E. (1962). On the linear theory of viscoelasticity. *Archive for Rational Mechanics and Analysis*, *11*, 291-356.

Haines, S. S., & Pride, S. R. (2006). Seismoelectric numerical modeling on a grid. *Geophysics*, *71*(6), N57–N65.

Haney, M. M., & Tsai, V. C. (2015). Nonperturbational surface-wave inversion: A Dix-type relation for surface waves. *Geophysics*, *80*, EN167–EN177.

Haney, M. M., & Tsai, V. C. (2017). Perturbational and nonperturbational inversion of Rayleigh-wave velocities. *Geophysics*, *82*, F15–F28.

Harmon, N., Wang, S., Rychert, C. A., Constable, S., & Kendall, J. M. (2021). Shear velocity inversion guided by resistivity structure from the PI-LAB experiment for integrated estimates of partial melt in the mantle. *Journal of Geophysical Research: Solid Earth*, *126*(8), e2021JB022202. doi: 10.1029/2021JB022202

Havlin, C., Holtzman, B. K., & Hopper, E. (2021). Inference of thermodynamic state in the asthenosphere from anelastic properties, with applications to North American upper mantle. *Phys. Earth Planet. Int.*, *314*, 106639.

Hawkins, R., Khalid, M., Smetana, K., & Trampert, J. (2023). Model order reduc-

tion for seismic waveform modelling: inspiration from normal modes. *Geophys. J. Int.*, *234*(3), 2255–2283.

Hopper, E., Gaherty, J. B., & Shillington, D. J. (2020). Preferential localized thinning of lithospheric mantle in the melt-poor Malawi Rift. *Nat. Geosci.*, *13*, 584–589. doi: 10.1038/s41561-020-0609-y

Hosseini, K., Matthews, K. J., Sigloch, K., Shephard, G. E., Domeier, M., & Tsekhmistrenko, M. (2018). Submachine: web-based tools for exploring seismic tomography and other models of Earth's deep interior. *Geochem. Geophys. Geosyst.*, *19*, 1464—1483.

Hoversten, G. M., Cassassuce, F., Gasperikova, E., Newman, G. A., Chen, J., Rubin, Y., ... Vasco, D. (2006). Direct reservoir parameter estimation using joint inversion of marine seismic AVA and CSEM data. *Geophysics*, *71*(3), C1–C13. doi: 10.1190/1.2194510

Hu, W., Abubakar, A., & Habashy, T. M. (2009). Joint electromagnetic and seismic inversion using structural constraints. *Geophysics*, *74*(6), R99–R109. doi: 10.1190/1.3246586

Huang, Y., & Schuster, G. (2012). Multisource least-squares migration of marine streamer and land data with frequency-division encoding. *Geophys. Prosp.*, *60*, 663–680.

Huang, Y., & Schuster, G. (2017). Multisource full waveform inversion of marine streamer data with frequency selection. *Geophys. Prosp.*, *66*, 1243–1257. doi: 10.1111/1365-2478.12588

Igel, H., Mora, P., & Riollet, B. (1995). Anisotropic wave propagation through finite-difference grids. *Geophysics*, *60*(4), 1203–1216.

IRIS. (2018, April). *Data services newsletter vol. 20, no. 1.* Retrieved 13 July 2023, from `https://ds.iris.edu/ds/newsletter/vol20/no1/`

Ivanov, A. G. (1939). Effect of electrization of Earth layers waves passing through them. *Doklady Akademii Nauk. SSSR*, *24*, 42–45.

Iyer, H. M., & Hirahara, K. (1993). *Seismic tomography, Theory and Practice.* Chapman & Hall.

Jackson, D. D. (1972). Interpretation of inaccurate, insufficient and inconsistent data. *Geophys. J. R. astr. Soc.*, *28*, 97–109.

Jardani, A., Revil, A., Slod, E., & Söllner, W. (2010). Stochastic joint inversion of

2D seismic and seismoelectric signals in linear poroelastic materials: A numerical investigation. *Geophysics*, *75*, N19–N31.

Kan, L. Y., Chevrot, S., & Monteiller, V. (2023). Dehydration of the subducting Juan de Fuca Plate and fluid pathways revealed by full waveform inversion of teleseismic P and SH waves in central Oregon. *J. Geophys. Res.: Solid Earth*, *128*, e2022JB025506.

Kanamori, H., & Anderson, D. L. (1977). Importance of physical dispersion in surface wave and free oscillation problems: Review. *Reviews of Geophysics*, *15(1)*, 105–112. doi: 10.1029/RG015i001p00105

Karaoğlu, H., & Romanowicz, B. (2018). Inferring global upper-mantle shear attenuation structure by waveform tomography using the spectral element method. *Geophys. J. Int.*, *213*, 1536–1558.

Karato, S.-I., & Jung, H. (1998). Water, partial melting and the origin of the seismic low velocity and high attenuation zone in the upper mantle. *Earth Planet. Sci. Lett.*, *157*, 193–207.

Karato, S.-I., & Karki, B. B. (2001). Origin of lateral variation of seismic wave velocities and density in the deep mantle. *J. Geophys. Res.*, *106*, 21771–21783. doi: 10.1029/2001JB000214

Kennett, B. L. N., Engdahl, E. R., & Buland, R. (1995). Constraints on seismic velocities in the Earth from traveltimes. *Geophys. J. Int.*, *122*, 108-124.

Kennett, B. L. N., & Sambridge, M. (1998). Inversion for multiple parameter classes. *Geophys. J. Int.*, *135*(1), 304-306. doi: 10.1046/j.1365-246X.1998.00657.x

Kennett, B. L. N., Widiyantoro, S., & van der Hilst, R. (1998). Joint seismic tomography for bulk-sound and shear wave speed in the Earth's mantle. *J. Geophys. Res.*, *103*, 12469–12493.

Komatitsch, D., & Tromp, J. (1999). Introduction to the spectral element method for three-dimensional seismic wave propagation. *Geophys. J. Int.*, *139*, 806–822.

Komatitsch, D., & Tromp, J. (2002). Spectral-element simulations of global seismic wave propagation, Part I: validation. *Geophys. J. Int.*, *149*, 390–412.

Komatitsch, D., & Vilotte, J. P. (1998). The spectral element method: an effective tool to simulate the seismic response of 2D and 3D geological structures. *Bull. Seism. Soc. Am.*, *88*, 368–392.

Krebs, J. R., Anderson, J. E., Hinkley, D., Neelamani, R., Lee, S., Baumstein, A., & Lacasse, M. (2009). Fast full-wavefield seismic inversion using encoded sources. *Geophysics*, *74*, WCC177–WCC188.

Krebs, J. R., Cha, Y., Lee, S., Dimitrov, P., Mullur, A., Downey, N., & Routh, P. (2013). Orthogonal source and receiver encoding. *US Patent Application (Patent 10,012,745)*.

Krischer, L., Fichtner, A., Zukauskaite, S., & Igel, H. (2015). Large-scale seismic inversion framework. *Seism. Res. Lett.*, *86*(4), 1198–1207. doi: 10.1785/0220140248

Kustowski, B., Ekström, G., & Dziewoński, A. M. (2008). Anisotropic shear-wave velocity structure of the Earth's mantle: A global model. *J. Geophys. Res. Solid Earth*, *113*(B6). doi: 10.1029/2007JB005169

Lailly, P. (1983). The seismic inverse problem as a sequence of before stack migration. In J. Bednar (Ed.), *Conference on inverse scattering: Theory and application* (pp. 206–220). SIAM.

Laske, G., & Masters, G. (1996). Constraints on global phase velocity maps from long-period polarization data. *J. Geophys. Res.*, *101*, 16059–16075.

Lau, H., Austermann, J., Mitrovica, J., Crawford, O., Al-Attar, D., & Latychev, K. (2018). Inferences of mantle viscosity based on ice age data sets: The bias in radial viscosity profiles due to the neglect of laterally heterogeneous viscosity structure. *J. Geophys. Res.*, *123*, 7237–7252.

Lebedev, S., Adam, J. M.-C., & Meier, T. (2013). Mapping the Moho with seismic surface waves: A review, resolution analysis, and recommended inversion strategies. *Tectonophysics*, *609*, 377–394.

Lebedev, S., Fullea, J., Xu, Y., & Bonadio, R. (2024). Seismic thermography. *Bull. Seis. Soc. Am.*, in press.

Lebedev, S., Grannell, J., Arroucau, P., Bonadio, R., Agostinetti, N. P., & Bean, C. J. (2023). Seismicity of Ireland, and why it is so low: How the thickness of the lithosphere controls intraplate seismicity. *Geophys. J. Int.*, *235*(1), 431–447.

Lebedev, S., & Nolet, G. (2003). Upper mantle beneath Southeast Asia from S velocity tomography. *J. Geophys. Res.*, *108*. doi: 10.1029/2000JB000073

Lei, W., Ruan, Y., Bozdağ, E., Peter, D., Lefebvre, M., Komatitsch, D., ... Pug-

mire, D. (2020). Global adjoint tomography—model GLAD-M25. *Geophys. J. Int.*, *223*(1), 1–21. doi: 10.1093/gji/ggaa253

Lekić, V., & Romanowicz, B. (2011). Inferring upper-mantle structure by full waveform tomography with the spectral-element method. *Geophys. J. Int.*, *185*, 799–831.

Leng, K. D., Korenaga, J., & Nissen-Meyer, T. (2020). 3-D scattering of elastic waves by small scale heterogeneities in the Earth's mantle. *Geophys. J. Int.*, *223*, 502–525.

Lévêque, J. J., Rivera, L., & Wittlinger, G. (1993). On the use of the checkerboard test to assess the resolution of tomographic inversions. *Geophys. J. Int.*, *115*, 313–318.

Li, X. B., & Romanowicz, B. (1996). Global mantle shear velocity model developed using nonlinear asymptotic coupling theory. *J. Geophys. Res.*, *101*, 11,245–22,271.

Lin, F.-C., Li, D., Clayton, R. W., & Hollis, D. (2013). High-resolution 3D shallow crustal structure in Long Beach, California: Application of ambient noise tomography on a dense seismic array. *Geophysics*, *78*, Q45–Q56.

Lin, F.-C., Tsai, V. C., & Schmandt, B. (2014). 3-D crustal structure of the western United States: application of Rayleigh-wave ellipticity extracted from noise cross-correlations. *Geophys. J. Int.*, *198*(2), 656–670.

Liu, Q., & Gu, Y. (2012). Seismic imaging: from classical to adjoint tomography. *Tectonophysics*, *566-567*, 31–66.

Liu, X. (2020). Finite-frequency sensitivity kernels for seismic noise interferometry based on differential time measurements. *J. Geophys. Res. Solid Earth*, *125*, e2019JB018932. doi: 10.1029/2019JB018932

Liu, Z., Hoffman, J., Simons, F. J., Tromp, J., Bachmann, E., & Cui, C. (2023). Laplace domain crosstalk-free source-encoded elastic full waveform inversion using time domain solvers. *Geophysics*. (Submitted)

Lv, M., Xu, X., Hu, S., Ding, Z., & Yao, P. (2024). Crustal deformation in eastern Himalayan syntaxis constrained by ambient noise tomography. *Bull. Seis. Soc. Am.*, in press.

Lyu, C., Zhao, L., Capdeville, Y., & Wei, Z. (2024). Error propagation and control in 2D and 3D hybrid seismic wave simulations for box tomography. *Bull. Seis.*

Soc. Am., in press.

Macchioli-Grande, F., Zyserman, F., Monachesi, L., Jouniaux, L., & Rosas-Carbajal, M. (2020). Bayesian inversion of joint SH seismic and seismoelectric data to infer glacier system properties. *Geophys. Prosp.*, *68*(5), 1633–1656.

Mahardika, H., Revil, A., & Jardani, A. (2012). Waveform joint inversion of seismograms and electrograms for moment tensor characterization of fracking events. *Geophysics*, *77*(5), ID23–ID39.

Mancini, F., Prindle, K., Ridsdill-Smith, T., & Moss, J. (2016). Full-waveform inversion as a game changer: Are we there yet? *The Leading Edge*, *35*(5), 445–451. doi: 10.1190/tle35050445.1

Marquering, H., Dahlen, F., & Nolet, G. (1999). Three-dimensional sensitivity kernels for finite-frequency traveltimes: the banana-doughnut paradox. *Geophys. J. Int.*, *137*, 805–815. doi: 10.1046/j.1365-246x.1999.00837.x

Martins Gomes, V. (2022). *Experimental characterization and modelling of electromagnetic waves generated by seismoelectric conversion at porous media interfaces.* (Theses, Université de Pau et des Pays de l'Adour). Retrieved from `https://theses.hal.science/tel-04136776`

Masson, Y. (2023). Distributional finite-difference modelling of seismic waves. *Geophys. J. Int.*, *233*, 264-296.

Masson, Y., & Romanowicz, B. (2017). Box Tomography: Localised imaging of remote targets buried in an unknown medium, a step forward for understanding key structures in the deep Earth. *Geophys. J. Int.*, *211*, 141–163.

Maupin, V., & Park, J. (2007). Wave propagation in anisotropic media. In B. Romanowicz & A. Dziewonski (Eds.), *Seismology and structure of the Earth* (Vol. 1, pp. 289–321). Elsevier.

McKenzie, D., Jackson, J., & Priestley, K. (2005). Thermal structure of oceanic and continental lithosphere. *Earth Planet. Sci. Lett.*, *233*, 337–349.

McNamara, A. K. (2019). A review of Large Low Shear Velocity Provinces and Ultra Low Velocity Zones. *Tectonophys.*, *760*, 199–220.

Mégnin, C., & Romanowicz, B. (2000). The 3D shear velocity structure of the mantle from the inversion of body, surface and higher modes wave forms. *Geophys. J. Int.*, *143*, 709–728.

Meyer, R.-C. (2021). *Mathematical modeling and simulation of waves in conducting*

poroelastic media using HDG method (Theses, Université de Pau et des Pays de l'Adour). Retrieved from `https://theses.hal.science/tel-03442300`

Mikhailov, O. V., Queen, J., & Toksöz, M. N. (2000). Using borehole electroseismic measurements to detect and characterize fractured (permeable) zones. *Geophysics*, *65*(4), 1098–1112.

Modrak, R. T., Borisov, D., Lefebvre, M., & Tromp, J. (2018). Seisflows—flexible waveform inversion software. *Computers & Geosciences*, *115*, 88–95. doi: 10.1016/j.cageo.2018.02.004

Monteiller, V., Chevrot, S., Komatitsch, D., & Fuji, N. (2013). A hybrid method to compute short-period synthetic seismograms of teleseismic body waves in a 3-D regional model. *Geophys. J. Int.*, *192*, 230–247.

Morency, C., Luo, Y., & Tromp, J. (2011). Acoustic, elastic and poroelastic simulations of CO_2 sequestration crosswell monitoring based on spectral-element and adjoint methods. *Geophys. J. Int.*, *185*, 955–966.

Morency, C., & Matzel, E. (2021). Seismic to electric conversion for carbon storage monitoring. In *Sixth International Conference on Engineering Geophysics, Virtual, 25–28 October 2021* (pp. 195–198).

Morency, C., Matzel, E., Grobbe, N., Brito, D., Bordes, C., Bernardo, N., ... Fagerås, B. (2022). Seismoelectric effects for geothermal resources assessment and monitoring: Overview and preliminary results. In *Proceedings, 47th Workshop on Getothermal Reservoir Engineering, Stanford University, Stanford, California, February 7-9, 2022* (p. SGP-TR-223).

Naif, S., Key, K., Constable, S., & Evans, R. L. (2013). Melt-rich channel observed at the lithosphere-asthenosphere boundary. *Nature*, *495*, 356–359.

Nakata, N., Chang, J. P., Lawrence, J. F., & Boué, P. (2015). Body wave extraction and tomography at Long Beach, California, with ambient-noise interferometry. *J. Geophys. Res.*, *120*, 1159–1173.

Neal, R. M. (2011). MCMC using Hamiltonian dynamics. In S. Brooks, A. Gelman, G. Jones, & X.-L. Meng (Eds.), *Handbook of Markov Chain Monte Carlo* (pp. 113–162). Chapman and Hall.

Nocedal, J., & Wright, S. J. (1999). *Numerical Optimization*. Springer, New York.

Nolet, G. (2008). *A Breviary of Seismic Tomography*. Cambridge University Press, Cambridge, UK.

1787 Nolet, G., & Dahlen, F. A. (2000). Wavefront healing and the evolution of seismic
1788 delay times. *J. Geophys. Res.*, *105*, 19043–19054.

1789 Nuzzo, R. (2014). Statistical errors. *Nature*, *506*, 150–152.

1790 Nyblade, A. A., Durrheim, R., Dirks, P., Graham, G., Gibson, R., & Webb, S.
1791 (2011). Geoscience initiative develops sustainable science in Africa. *Eos*
1792 *Trans. AGU*, *92*, https://doi.org/10.1029/2011EO190002.

1793 Obayashi, M., Yoshimitsu, J., Nolet, G., Fukao, Y., Shiobara, H., Sugioka, H., ...
1794 Gao, Y. (2013). Finite frequency whole mantle P wave tomography: Improve-
1795 ment of subducted slab images. *Geophys. Res. Lett.*, *40*(21), 5652–5657. doi:
1796 10.1002/2013GL057401

1797 Okaya, D., Rabbel, W., Beilecke, T., & Hasenclever, J. (2004). P wave material
1798 anisotropy of a tectono-metamorphic terrane: An active source seismic exper-
1799 iment at the KTB super-deep drill hole, southeast Germany. *Geophys. Res.*
1800 *Lett.*, *31*. doi: 10.1029/2004GL020855

1801 Oldenburg, D. W. (1974). The inversion and interpretation of gravity anomalies.
1802 *Geophysics*, *39*, 526–536.

1803 Park, S., Avouac, J.-P., Zhan, Z., & Gualandi, A. (2023). Weak upper-mantle base
1804 revealed by postseismic deformation of a deep earthquake. *Nature*, *615*, 455–
1805 460.

1806 Pavlis, G. L., & Booker, J. R. (1980). The mixed discrete-continuous inverse prob-
1807 lem: Application to the simultaneous determination of earthquake hypocenters
1808 and velocity structure. *J. Geophys. Res. Solid Earth*, *85*, 4801–4810. doi:
1809 10.1029/JB085iB09p04801

1810 Perugu, M., Sribin, C., Dewangan, P., Yatheesh, V., & Gupta, S. (2024). 3-
1811 dimensional local earthquake tomography of the Andaman-Nicobar subduction
1812 zone using ocean bottom seismometer data. *Bull. Seis. Soc. Am.*, in press.

1813 Pienkowska, M., Monteillier, V., & Nissen-Meyer, T. (2021). High-frequency global
1814 wavefields for local 3-D structures by wavefield injection and extrapolation.
1815 *Geophys. J. Int.*, *223*, 1782–1798.

1816 Pipatprathanporn, S., & Simons, F. J. (2022). One year of sound recorded
1817 by a MERMAID float in the Pacific: Hydroacoustic earthquake signals
1818 and infrasonic ambient noise. *Geophys. J. Int*, *228*, 193—212. doi:
1819 10.1093/gji/ggab296

Pladys, A., Brossier, R., Li, Y., & Metivier, L. (2021). On cycle-skipping and misfit function modification for full-wave inversion: Comparison of five recent approaches. *Geophysics*, *86*, R563–R587.

Powell, E., Gomez, N., Hay, C., Latychev, K., & Mitrovica, J. (2020). Viscous effects in the solid Earth response to modern Antarctic ice mass flux: Implications for geodetic studies of WAIS stability in a warming world. *J. Clim.*, *33*, 443–459.

Pride, S. R. (1994). Governing equations for the coupled electromagnetics and acoustics of porous media. *Physical Review B*, *50*, 15,678–15,696.

Priestley, K., Ho, T., Takei, Y., & McKenzie, D. (2024). The thermal and anisotropic structure of the top 300 km of the mantle. *Earth Planet. Sci. Lett.*, *626*, doi:10.1016/j.epsl.2023.118525.

Priestley, K., & McKenzie, D. (2006). The thermal structure of the lithosphere from shear wave velocities. *Earth Planet. Sci. Lett.*, *244*, 285–301.

Priestley, K., & McKenzie, D. (2013). The relationship between shear wave velocity, temperature, attenuation and viscosity in the shallow part of the mantle. *Earth Planet. Sci. Lett.*, *381*, 78–91.

Quarteroni, A., Manzoni, A., & Negri, F. (2016). *Reduced basis methods for partial differential equations: An introduction*. Springer.

Resovsky, J., & Trampert, J. (2002). Reliable mantle density error bars: an application of the Neighbourhood Algorithm to normal-mode and surface wave data. *Geophys. J. Int.*, *150*(3), 665–672.

Revil, A., & Jardani, A. (2010). Seismoelectric response of heavy oil reservoirs: theory and numerical modelling. *Geophys. J. Int.*, *180*, 781–797.

Ringler, A. T., Anthony, R. E., Aster, R. C., Ammon, C. J., Arrowsmith, S., Benz, H., ... Yeck, W. (2022). Achievements and prospects of global broadband seismographic networks after 30 years of continuous geophysical observations. *Rev. Geophys.*, *60*, doi:10.1029/2021RG000749.

Ritsema, J., & Lekić, V. (2020). Heterogeneity of seismic wave velocity in Earth's mantle. *Annu. Rev. Earth Planet. Sci.*, *48*, 377-–401. doi: 10.1146/annurev-earth-082119-065909

Ritsema, J., Rivera, L. A., Komatitsch, D., Tromp, J., & van Heijst, H.-J. (2002). Effects of crust and mantle heterogeneity on pp/p and ss/s amplitude ratios. *Geophys. Res. Lett.*, *29*(10), 72-1–72-4. doi: 10.1029/2001GL013831

Ritsema, J., & van Heijst, H. J. (2002). Constraints on the correlation of P- and S-wave velocity heterogeneity in the mantle from P, PP, PPP and PKPab traveltimes. *Geophys. J. Int.*, *149*, 482–489.

Robertson, G. S., & Woodhouse, J. H. (1996). Ratio of relative S to P velocity heterogeneity in the lower mantle. *J. Geophys. Res.*, *101*. doi: 10.1029/96JB01905

Robson, A., Lau, H. C. P., Koelemeijer, P., & Romanowicz, B. (2022). An analysis of core–mantle boundary Stoneley mode sensitivity and sources of uncertainty. *Geophys. J,. Int.*, *228*, 1962–1974. doi: 10.1093/gji/ggab448

Rodgers, A., Krischer, L., Afanasiev, A., Boehm, C., Doody, C., & Simmons, N. (2024). Adjoint waveform tomography for crustal and upper mantle structure of the Middle East and Southwest Asia for improved waveform simulations using openly available broadband data. *Bull. Seis. Soc. Am.*, in press.

Rodgers, A., Krischer, L., Afanasiev, M., Boehm, C., Doody, C., Chiang, A., & Simmons, N. (2022). WUS256: An adjoint waveform tomography model of the crust and upper mantle of the western United States for improved waveform simulations. *J Geophys. Res.: Solid Earth*, *127*(7), e2022JB024549. doi: 10.1029/2022JB024549

Romanowicz, B. (2023). Global seismic tomography using time-domain waveform inversion. In *Applications of Data Assimilation and Inverse Problems in the Earth Sciences* (pp. 220–234).

Romanowicz, B., & Mitchell, B. J. (2015). Deep Earth structure - Q of the Earth from Crust to Core. In A. Dziewonski & B. Romanowicz (Eds.), *Treatise on Geophysics* (pp. 789–827). Elsevier.

Romero, L., Ghiglia, D., Ober, C., & Morton, S. (2000). Phase encoding of shot records in prestack migration. *Geophysics*, *65*, 426—436.

Rozza, G., Huynh, D., & Patera, A. (2008). Reduced basis approximation and a posteriori error estimation for affinely parametrized elliptic coercive partial differential equations: application to transport and continuum mechanics. *Arch. Comput. Meth. Eng.*, *15*, 229—275.

Sager, K., Boehm, C., Ermert, L., Krischer, L., & Fichtner, A. (2020). Global-scale full-waveform ambient noise inversion. *J. Geophys. Res.*, *125*. doi: 10.1029/2019JB018644

Sambridge, M. S., Gallagher, K., Jackson, A., & Rickwood, P. (2006). Trans-dimensional inverse problems, model comparison, and the evidence. *Geophys. J. Int.*, *167*, 528–542.

Santosa, F., & Symes, W. W. (1988). Computation of the Hessian for least-squares solutions of inverse problems of reflection seismology. *Inverse Problems*, *4*, 211–233.

Schiemenz, A., & Igel, H. (2013). Accelerated 3-D full-waveform inversion using simultaneously encoded sources in the time domain: Application to Valhall ocean-bottom cable data. *Geophys. J. Int.*, *195*, 1970–1988.

Schuster, G., Wang, X., Huang, Y., Dai, W., & Boonyasiriwat, C. (2011). Theory of multisource crosstalk reduction by phase-encoded statics. *Geophys. J. Int.*, *184*, 1289–1303.

Shinevar, W. J., Golos, E. M., Jagoutz, O., Behn, M. D., & van der Hilst, R. D. (2023). Mantle thermochemical variations beneath the continental United States through petrologic interpretation of seismic tomography. *Earth Planet. Sci. Lett.*, *602*, 117965. doi: 10.1016/j.epsl.2022.117965

Shinevar, W. J., Jagoutz, O., & Behn, M. D. (2022). WISTFUL: Whole-Rock Interpretative Seismic Toolbox for Ultramafic Lithologies. *Geochem., Geophys., Geosyst.*, *23*(8), e2022GC010329. doi: 10.1029/2022GC010329

Sieminski, A., Trampert, J., & Tromp, J. (2009). Principal component analysis of anisotropic finite-frequency kernels. *Geophys. J. Int.*, *179*, 1186–1198.

Simons, F. J., Simon, J. D., & Pipatprathanporn, S. (2021). Twenty-thousand leagues under the sea: Recording earthquakes with autonomous floats. *Acoustics Today*, *17*(2), 42–51.

Spencer, C., & Gubbins, D. (1980). Travel-time inversion for simultaneous earthquake location and velocity structure determination in laterally varying media. *Geophys. J. Int.*, *63*, 95–116. doi: 10.1111/j.1365-246X.1980.tb02612.x

Spetzler, J., & Snieder, R. (2001). The effect of small scale heterogeneity on the arrival time of waves. *Geophys. J. Int.*, *145*, 786–796.

Staehler, S. C., Sigloch, K., & Nissen-Meyer, T. (2012). Triplicated P-wave measurements for waveform tomography of the mantle transition zone. *Solid Earth*, *3*. doi: 10.5194/se-3-339-2012

Stanzione, D., West, J., Evans, R., Minyard, T., Ghattas, O., & Panda, D. (2020,

7). Frontera: The Evolution of Leadership Computing at the National Science Foundation. In (pp. 106–111). doi: 10.1145/3311790.3396656

Suetsugu, D., & Shiobara, H. (2014). Broadband ocean bottom seismology. *Ann. Rev. Earth Planet. Sci.*, *42*, 27–43.

Sukhovich, A., Bonnieux, S., Hello, Y., J.-O.Irisson, Simons, F., & Nolet, G. (2015). Long-awaited mathematics proof could help scan Earth's innards. *Nat. Commun.*, *6*, 8027–8033.

Tanaka, H. K. M., Uchida, T., Tanaka, M., Shinohara, H., & Taira, H. (2009). Cosmic-ray muon imaging of magma in a conduit: degassing process of Satsuma-Iwojima volcano, Japan. *Geophys. Res. Lett.*, *36*, L01304.

Tao, K., Grand, S. P., & Niu, F. (2018). Seismic structure of the upper mantle beneath eastern Asia from full waveform seismic tomography. *Geochemistry, Geophysics, Geosystems*, *19*(8), 2732–2763. doi: 10.1029/2018GC007460

Tape, C., Liu, Q., Maggi, A., & Tromp, J. (2009). Adjoint tomography of the southern California crust. *Science*, *325*, 988–992.

Tape, C., Liu, Q., Maggi, A., & Tromp, J. (2010). Seismic tomography of the southern California crust based upon spectral-element and adjoint methods. *Geophys. J. Int.*, *180*, 433–462.

Tape, W., & Tape, C. (2022). Two complementary methods of inferring elastic symmetry. *J. Elasticity*, *150*, 91–118. doi: 10.1007/s10659-022-09898-0

Tarantola, A. (1984). Inversion of seismic reflection data in the acoustic approximation. *Geophysics*, *49*(8), 1259–1266.

Tarantola, A., & Valette, B. (1982). Generalized nonlinear inverse problems solved using the least squares criterion. *Rev. Geophys.*, *20*, 219–232.

Thompson, A. H., & Gist, G. A. (1993). Geophysical applications of electrokinetic conversion. *The Leading Edge*, *December*, 1169–1173.

Thrastarson, S., van Driel, M., Krischer, L., Boehm, C., Afanasiev, M., van Herwaarden, D.-P., & Fichtner, A. (2020). Accelerating numerical wave propagation by wavefield adapted meshes, Part II: Full-waveform inversion. *Geophys. J. Int.*, *221*, 1591–1604.

Thrastarson, S., van Herwaarden, D.-P., Krischer, L., & Fichtner, A. (2021). LASIF: Large-Scale Seismic Inversion Framework: An updated version. *Earth ArXiv*. doi: doi:10.31223/X5NC84

Thrastarson, S., van Herwaarden, D.-P., Noe, S., Schiller, C., & Fichtner, A. (2024). REVEAL: A global full-waveform inversion model. *Bull. Seis. Soc. Am.*, in press.

Thurber, C., & Eberhart-Phillips, D. (1999). Local earthquake tomography with flexible gridding. *Computers & Geosciences*, *25*, 809–818. doi: 10.1016/S0098-3004(99)00007-2

Tong, P., Chen, C. W., Komatitsch, D., Basini, P., & Liu, Q. Y. (2014). High-resolution seismic array imaging based on an SEM-FK hybrid method. *Geophys. J. Int.*, *197*(1), 369–395.

Tromp, J. (2020). Seismic wavefield imaging of Earth's interior across scales. *Nature Rev. Earth Environ.*, 40–53. doi: 10.1038/s43017-019-0003-8

Tromp, J., & Bachmann, E. (2019). Source encoding for adjoint tomography. *Geophys. J. Int.*, *218*, 2019–2044.

Tromp, J., Tape, C., & Liu, Q. (2005). Seismic tomography, adjoint methods, time reversal and banana-doughnut kernels. *Geophys. J. Int.*, *160*, 195–216. doi: 10.1111/j.1365-246X.2004.02453.x

Tsai, V. C. (2023). The future of Earth imaging. *Seis. Res. Lett.*, *94*, 2119–2128. doi: 10.1785/0220230125

Tsai, V. C., Huber, C., & Dalton, C. A. (2023). Towards the geological parametrization of seismic tomography. *Geophys. J. Int*, *234*, 1447–1462. doi: 10.1093/gji/ggad140

Tsekhmistrenko, M., Sigloch, K., Hosseini, K., & Barruol, G. (2021). A tree of Indo-African mantle plumes imaged by seismic tomography. *Nat. Geosc.*, *14*, doi:ff10.1038/s41561-021-00762-9.

van der Wal, W., Whitehouse, P. L., & Schrama, E. J. (2015). Effect of GIA models with 3D composite mantle viscosity on GRACE mass balance estimates for Antarctica. *Earth Planet. Sci. Lett.*, *414*, 134–143.

van Herwaarden, D.-P., Boehm, C., Afanasiev, M., Thrastarson, S., Krischer, L., van Driel, M., & Fichtner, A. (2020). Accelerated full-waveform inversion using dynamic mini-batches. *Geophys. J. Int.*, *221*, 1427–1438.

Vehtari, A., Gelman, A., & Gabry, J. (2017). Practical Bayesian model evaluation using leave-one-out cross validation and WAIC. *Stat. Comput.*, *27*, 1413–1432.

Virieux, J., Asnaashari, A., Brossier, R., Metivier, L., Ribodetti, A., & Zhou, W.

(2017). An introduction to full-waveform inversion. *Encyclopedia of Exploration Geophysics*, doi:10.1190/1.9781560803027.entry6.

Virieux, J., & Operto, S. (2009). An overview of full-waveform inversion in exploration geophysics. *Geophysics*, *74*, WCC1–WCC26.

Volterra, V. (2005). *Theory of functionals and of integral and integro-differential equations*. Dover Publications, New York.

Wang, K., Liu, Q., & Yang, Y. (2019). Three-dimensional sensitivity kernels for multicomponent empirical Green's functions from ambient noise: Methodology and application to adjoint tomography. *J. Geophys. Res. Solid Earth*, *124*, 5794–5810. doi: 10.1029/2018JB017020

Wang, K., Yang, Y. J., Jiang, C. X., Wang, Y., Tong, P., Liu, T. S., & Liu, Q. Y. (2021). Adjoint tomography of ambient noise data and teleseismic P waves: Methodology and applications to central California. *J. Geophys. Res*, *126*(6), e2021JB021648.

Wang, Y., Chevrot, S., Monteiller, V., Komatitsch, D., Mouthereau, F., Manatschal, G., ... Martin, R. (2016). The deep roots of the western Pyrenees revealed by full waveform inversion of teleseismic P waves. *Geology*, *44*, 475–478.

Wang, Y., Lin, F.-C., & Ward, K. M. (2019). Ambient noise tomography across the cascadia subduction zone using dense linear seismic arrays and double beamforming. *Geophys. J. Int.*, *217*(3), 1668–1680.

Wasserstein, R. L., & Lazar, N. A. (2016). The ASA's statement on p-values: context, process, and purpose. *Am. Stat.*, *70*, 129-133.

Widmer, R., Masters, G., & Gilbert, F. (1991). Spherically symmetric attenuation within the Earth from normal mode data. *Geophys. J. Int.*, *104*, 541–553.

Wilgus, J., Schmandt, B., Maguire, R., Jiang, C., & Chaput, J. (2023). Shear velocity evidence of upper crustal magma storage beneath valles caldera. *Geophys. Res. Lett.*, *50*(5), e2022GL101520.

Woodhouse, J. H., & Dziewoński, A. M. (1984). Mapping the upper mantle: Three-dimensional modeling of Earth structure by inversion of seismic waveforms. *J. Geophys. Res. Solid Earth*, *89*, 5953–5986. doi: 10.1029/JB089iB07p05953

Woodhouse, J. H., & Wong, Y. (1986). Amplitude, phase and path anomalies of mantle waves. *Geophys. J. R. Astr. Soc.*, *87*, 753–773.

Xu, M. J., Wang, K., Chen, J., Yu, D. Y., & Tong, P. (2023). Three-dimensional

receiver function adjoint tomography for high-resolution seismic array imaging: Methodology and applications in southeastern Tibet. *J. Geophys. Res.*, submitted.

Yang, X., & Gao, H. (2020). Segmentation of the Aleutian-Alaska subduction zone revealed by full-wave ambient noise tomography: Implications for the along-strike variation of volcanism. *J. Geophys. Res.*, *125*(11), e2020JB019677.

Yang, Y., & Engquist, B. (2018). Analysis of optimal transport and related misfit functions in full-waveform inversion. *Geophysics*, *83*, A7–A12.

Yoshizawa, K., & Kennett, B. L. N. (2002). Determination of the influence zone for surface wave paths. *Geophys. J. Int.*, *149*, 440–453.

Yuan, S., & Xu, W. (2019). The new progress of China Array project. *Geophys. Res. Abstr., EGU General Assembly*, *21*, https://meetingorganizer.copernicus.org/EGU2019/EGU2019-180.

Yuan, Y. O., Simons, F. J., & Tromp, J. (2016). Double-difference adjoint seismic tomography. *Geophys. J. Int.*, *206*, 1599–1618. doi: 10.1093/gji/ggw233

Zenonos, A., De Siena, L., Widiyantoro, S., & Rawlinson, N. (2019). P and S wave travel time tomography of the SE Asia-Australia collision zone. *Phys. Earth Planet. Inter.*, *293*, 106267. doi: 10.1016/j.pepi.2019.05.010

Zhang, H., & Thurber, C. (2003). Double-difference tomography: The method and its application to the Hayward Fault, California. *Bull. Seism. Soc. Am.*, *93*, 1875–1889. doi: 10.1785/0120020190

Zhang, Q., Mao, W., Zhou, H., Zhang, H., & Chen, Y. (2018). Hybrid-domain simultaneous-source full waveform inversion without crosstalk noise. *Geophys. J. Int.*, *215*, 1659–1681.

Zhang, X., & Curtis, A. (2020). Seismic tomography using variational inference methods. *J. Geophys. Res. Solid Earth*, *125*(4), e2019JB018589. doi: 10.1029/2019JB018589

Zhang, X., Lomas, A., Zhou, M., Zheng, Y., & Curtis, A. (2022). 3-D Bayesian variational full waveform inversion. *Geophys. J. Int.*, *234*, 546–561.

Zhao, D., Wang, J., Huang, Z., & Liu, X. (2021). Seismic structure and subduction dynamics of the western Japan arc. *Tectonophysics*, *802*, 228743. doi: 10.1016/j.tecto.2021.228743

Zhao, L., Jordan, T. H., & Chapman, C. H. (2000). Three-dimensional Fréchet dif-

ferential kernels for seismic delay times. *Geophys. J. Int.*, *141*, 558–576. doi: 10.1046/j.1365-246x.2000.00085.x

Zhao, Z., Sen, M., & Stoffa, P. (2016). Double-plane-wave reverse time migration in the frequency domain. *Geophysics*, *81(5)*, S367–S382.

Zhou, Z., Gerstoft, P., & Olsen, K. B. (2024). 3D multiresolution velocity model fusion with probability graphical models. *Bull. Seis. Soc. Am.*, in press.

Zhu, H., Bozdağ, E., & Tromp, J. (2015, 02). Seismic structure of the European upper mantle based on adjoint tomography. *Geophys. J. Int.*, *201*(1), 18–52.

Mailing addresses of authors

Andreas Fichtner: Department of Earth Sciences, ETH Zurich, Sonneggstrasse 5, 8092 Zurich, Switzerland.

Brian L. N. Kennett: Research School of Earth Sciences, The Australian National University, Canberra, Australia

Victor C. Tsai: Department of Earth, Environmental and Planetary Sciences, Brown University, Providence RI, USA

Clifford H. Thurber: Department of Geoscience, University of Wisconsin-Madison, Madison, WI, USA

Arthur J. Rodgers and Christina Morency: Lawrence Livermore National Laboratory, Livermore, CA, USA

Carl Tape: University of Alaska Fairbanks, Fairbanks, AK, USA

Nicholas Rawlinson, Sergei Lebedev and Keith Priestley: Department of Earth Sciences, University of Cambridge, Cambridge, United Kingdom

Ebru Bozdag: Department of Applied Mathematics & Statistics and Department of Geophysics, Colorado School of Mines, Golden, CO, USA

Roger D. Borcherdt: U. S. Geological Survey, Menlo Park, CA, USA

Jeroen Tromp: Department of Geosciences and Program in Applied & Computational Mathematics, Princeton17 University, Princeton, NJ, USA

Jeroen Ritsema: Earth & Environmental Sciences, University of Michigan Ann Arbor, MI, USA

Barbara Romanowicz: Department of Earth and Planetary Science, University of California at Berkeley, Berkeley, CA, USA

Qinya Liu: Department of Physics & Department of Earth Sciences, University of Toronto, Toronto, Canada

Fan-Chi Lin: Department of Geology and Geophysics, University of Utah, Salt Lake City, UT, USA

Figure captions

Figure 1. Illustration of the Fang et al. (2016) model discretization (a) Horizontal plane: The black solid line represents the propagation path between two stations A and B for the surface wave at some period. The phase slowness at any point p along the path is determined from the values at four surrounding horizontal grid points (1-4) using bilinear interpolation. (b) Vertical direction:The vertical grid model (bigger black dots with finer layers shown as the black line) is perturbed (as shown by the red dot and red dashed lines) to compute the depth sensitivity of dispersion data to model parameters via differences. Modified from Fang et al. (2016).

Figure 2. Map view of part of a velocity grid across New Zealand, showing an example of the box for computing group velocity (U) partial derivatives at points (red dots) in a volume surrounding a U observation (yellow star), analogous to points along a path from an earthquake travel time. Small dots are 3D velocity grid nodes; stars are U observation locations (nodes of U velocity map). From Eberhart-Phillips and Fry (2017).

Figure 3. Effect of upper-mantle attenuation on vertical-component minor- and major-arc Rayleigh waves (right panel) where the corresponding ray paths are shown top left. Simulations are performed for the 3D mantle model GLAD-M25 (Lei et al., 2020) with 1D Q model QL6 (Durek & Ekström, 1996) (blue) and with QM1 (Widmer et al., 1991) in the upper mantle (red) as shown bottom left. Seismograms were computed by the 3D global wave propagation solver SPECFEM3D_GLOBE (Komatitsch & Tromp, 2002) and filtered between 40-250 s. Figure courtesy Ridvan Örsvuran.

Figure 4. (a) The degree-12 Vs structure S12 – similar to other global-scale tomographic Vs models for the mantle (e.g., Ritsema & Lekic, 2020) – along a great circle through the southwestern Pacific region on the left and North America on the right. The star indicates the hypocenter of an earthquake beneath Tonga-Fiji. The triangle is at an epicentral distances of $120\circ$. (b) Spectral-element-method (Komatitsch & Tromp, 1999) waveforms of the P and SH wave for a distance of 120°, computed for (dashed lines) PREM (Dziewonski & Anderson, 1981) and (solid lines) S12 and P12. P12 differs from S12 by a scaling factor R that increases from

1 in the upper mantle to 3 in the lower mantle, consistent with global travel time measurements (e.g., Robertson & Woodhouse, 1996; Ritsema & van Heijst, 2002). The numbers on the right indicate the misalignment between the S12/P12 and PREM signals. The P wave's deceleration in the LLVP and its acceleration in the Farallon anomaly and the lithosphere of eastern North America are equal so the P-wave arrival time is the same as the PREM predicted arrival time. This figure is a modification of Figure 9 in Chaves et al. (2020).

Figure 5. Box Tomography set up for imaging of a remote target region in the Earth. The Green's functions (1) and (3) are pre-computed in a reference global model and recorded at the boundaries of the target region. FWI proceeds with wavefield computations restricted to the target region (2). Time reversal mirrors allow the reconstruction of the full wavefield from the remote source to the remote station, at each iteration.

Figure 6. An elastic map $\mathbf{T}$ and a closest map $\mathbf{K}_\Sigma$ to it having symmetry Σ (trivial, monoclinic, orthorhombic, tetragonal, trigonal, cubic, transverse isotropic, isotropic). Each map $\mathbf{K} = \mathbf{K}_\Sigma$ is depicted as the contour map of its "monoclinic angle function" $\alpha^{\mathbf{K}}_{\mathrm{MONO}}$ (W. Tape & Tape, 2022). For a point $\mathbf{v}$ on the sphere, $\alpha^{\mathbf{K}}_{\mathrm{MONO}}(\mathbf{v})$ is the angle between $\mathbf{K}$ and the closest elastic map to $\mathbf{K}$ having a 2-fold symmetry axis at $\mathbf{v}$. The green points are where $\alpha^{\mathbf{K}}_{\mathrm{MONO}} = 0$ (inconsistent with the color scale) and are therefore the 2-fold axes of $\mathbf{K}$. They determine the symmetry group of $\mathbf{K}$, which is also seen in the contour plot itself. In this example, $\mathbf{T}$ has trivial symmetry and is from Igel et al. (1995); it is $\beta = 4.3°$ from being monoclinic and is $\beta = 30.6°$ from being isotropic.